Astron. Astrophys. 313, 25–44 (1996)

ASTRONOMY AND ASTROPHYSICS

A powerful radio galaxy at $z = 3.6$ in a giant rotating Lyman α halo*

R. van Ojik[1], H.J.A. Röttgering[1,2,3], C.L. Carilli[1,4], G.K. Miley[1], M.N. Bremer[1], and F. Macchetto[5,6]

[1] Leiden Observatory, P.O. Box 9513, 2300 RA, Leiden, The Netherlands
[2] Mullard Radio Astronomy Observatory, Cavendish Laboratory, Cambridge CB3 0HE, England
[3] Institute of Astronomy, Madingley Road, Cambridge CB3 0HA, England
[4] Harvard-Smithsonian Center for Astrophysics, Cambridge, MA 02138, USA
[5] Space Telescope Science Institute, 3700 San Martin Drive, Baltimore MD 21218, USA
[6] Affiliated with the Space Science Department of ESA

Received 27 April 1995 / Accepted 29 November 1995

Abstract. We present the discovery and detailed observations of the radio galaxy 1243+036 at a redshift of $z = 3.57$. The radio source was selected on the basis of its extremely steep radio spectrum, suggesting that it might be very distant. The radio source was identified with a galaxy of R magnitude 22.5. Subsequent spectroscopy showed strong Lyman α and [O III]$\lambda\lambda$5007,4959 emission, indicating that the object is a radio galaxy at $z = 3.57$. High resolution (0.2″) radio maps show an FRII type radio source with a sharply bent radio structure. Strong depolarization of the radio emission indicates that the source is embedded in a magneto-ionic medium.

The most spectacular feature of 1243+036 is the presence of a Lyα halo of luminosity $\sim 10^{44.5}$ erg s^{-1} which extends over $\sim 20''$ (135 kpc). A 0.6″ resolution Lyα image shows that the emission line gas is aligned with the main axis of the radio source and has structure down to the scale of the resolution. High resolution spectra show that the Lyα emitting gas has complex kinematic structure. The gas contained within the radio structure has a relatively high velocity width ($\sim$1500 km s^{-1} FWHM). The component of the Lyα emission that coincides with the bend in the radio structure is blueshifted with respect to the peak of the emission by 1100 km s^{-1}. There is low surface brightness Lyα emission aligned with, but extending 40 kpc beyond both sides of the radio source. This halo has a narrow velocity width ($\sim$250 km s^{-1} FWHM) and a velocity gradient of 450 km s^{-1} over the extent of the emission.

The presence of the quiescent Lyα component aligned with the AGN axis, but outside the radio source, is strong evidence that photoionization by anisotropically emitted radiation from the active nucleus is occurring. Various mechanisms for the origin and kinematics of the Lyα halo are discussed. Because the halo extends beyond the radio structure with less violent and more ordered kinematics than inside the radio structure, we conclude that the outer halo and its kinematics must predate the radio source. The ordered motion may be large-scale rotation caused by the accretion of gas from the environment of the radio galaxy or by a merger. Although alternatively the halo may be caused by a massive outflow, we argue that bulk inflow of the emission line gas is inconsistent with the most likely orientation of the radio source.

The large velocity-width of the Lyα gas contained within the radio source compared to that of the outer halo suggest a direct interaction of the radio source with the gas. The spatial correlation of enhanced, blue-shifted Lyα emission and the sharp bend of the radio structure suggest that the emission line gas could have deflected the radio jet. The impact of the jet could have accelerated the gas at this position and may have locally enhanced the Lyα emission.

Extended faint optical continuum emission is aligned with the principal radio axis, a phenomenon commonly observed in high redshift radio galaxies. This emission does not follow the bending of the radio jet, indicating that, at least in 1243+036, models invoking scattering of continuum radiation from the AGN as the cause of this alignment are favoured.

Key words: galaxies: active – galaxies: individual: 1243+036 – radio continuum: galaxies: – galaxies: kinematics and dynamics – cosmology: observations

1. Introduction

Finding galaxies at large redshifts is important for our understanding of galaxy formation in the early Universe. Se-

Send offprint requests to: H.J.A. Röttgering

* Based on observations collected at the European Southern Observatory, La Silla, Chile, and at the Very Large Array. The VLA is a facility of the U.S. National Radio Astronomy Observatory, which is operated by Associated Universities, Inc., under cooperative agreement with the U.S. National Science Foundation

lecting ultra steep spectrum radio sources ($\alpha < -1$, see Sect. 2) has proven to be the most efficient way of finding distant galaxies (e.g. Chambers et al. 1990; McCarthy 1993). Searches based on this method have resulted in the discovery of many high redshift ($z > 2$) radio galaxies (HZRGs), but few with $z > 3$ (Lilly 1988, Chambers et al. 1990, McCarthy et al. 1990b, Eales et al. 1993a, Röttgering 1993). In the last few years, we have carried out a programme to enlarge the sample of HZRGs, by selecting ultra steep spectrum (USS) radio sources (e.g. Röttgering 1993). This project has included radio imaging (Röttgering et al. 1994), optical broadband imaging (Röttgering et al. 1995b) and spectroscopy of potential distant galaxies. The optical observations were carried out as a Key Programme at the European Southern Observatory in Chile. Our USS radio source survey has resulted in the discovery of 29 radio galaxies at redshifts $z > 2$ (Röttgering 1993, van Ojik et al. 1994, Röttgering et al. 1996). We have now started follow up observations to study individual objects in more detail. This includes high resolution spectroscopy and narrow band imaging of the Lyα emitting gas, infrared spectroscopy and a sensitive high resolution radio survey of the objects. Here we report on the most distant galaxy discovered in the ESO Key Programme, 1243+036 (=4C 03.24) at $z = 3.57$. This is one of the most distant galaxies reported until now and its redshift is only exceeded by 4C 41.17 at $z = 3.8$ (Chambers et al. 1990) and 8C1435+63 at $z = 4.25$ (Lacy et al. 1994).

In Sect. 2 we describe the selection of the object, the observations and data analysis. In Sect. 3 the observational results are presented and physical parameters are deduced. Subsections describe the determination of the redshift and the kinematics of the Lyα gas (3.1), the properties of the radio source (3.2), the morphology of the optical continuum and Lyα emission (3.3) and a summary of the various radio and optical components (3.5). In Sect. 4 we discuss the observed characteristics of 1243+036 and in particular the kinematics of the ionized gas. We discuss the ionization and density of the Lyα gas (4.1), the kinematics of the ionized gas and scenarios for the origin of the outer halo (4.2), the bent radio structure and its relation to the ionized gas (4.3) and the aligned optical continuum emission (4.4). We summarize our conclusions in Sect. 5.

Throughout this paper we assume a Hubble constant of $H_0 = 50\,\mathrm{km\,s^{-1}\,Mpc^{-1}}$ and a deceleration parameter of $q_0 = 0.5$.

2. Selection and observations

As a basis for our survey to find distant galaxies, several radio catalogues at different frequencies and different overlapping regions of the sky were combined to select samples of USS (radio spectral index $\alpha < -1$, where $S_\nu \propto \nu^\alpha$, with S_ν the flux density and ν the frequency) radio sources (Röttgering et al. 1994). The samples were selected at a range of frequencies from 38 MHz to 408 MHz. The radio galaxy 1243+036 is part of the 178 MHz selected sample (Röttgering et al. 1994), and is also known as 4C 03.24. The samples of USS sources were then observed with the VLA as a preliminary for optical imaging and spectroscopy (Röttgering et al. 1994).

The 1.5″ resolution VLA image of 1243+036 from Röttgering et al. (1994) at 1465 MHz shows a simple, although bent, double morphology, with a full angular extent of 8″. The source has a total flux density at 1.5 GHz of 310 mJy, and has a very steep integrated radio spectrum, with a spectral index, α, between 178 MHz and 2700 MHz of -1.3. 1243+036 was optically identified from R-band CCD imaging of these samples of radio sources using the ESO-MPI 2.2 m telescope. These observations are described in Röttgering et al. (1995b) .

Here we describe low resolution spectroscopic observations to determine the redshift of 1243+036 and follow up observations using high resolution spectroscopy and imaging of the Lyα gas and the radio source to study the radio galaxy in more detail. A summary of the various observations is given in Table 1.

2.1. Optical spectroscopy

2.1.1. Low resolution

Low resolution optical spectroscopy was carried out on the ESO New Technology Telescope (NTT), using the ESO Multi-Mode Instrument (EMMI). The detector was a Thomson CCD with 1024^2 pixels that has a scale along the slit of 0.37″ per pixel. The spectrum covered the wavelength region from 4100 Å to 7900 Å. A 2″ wide slit was used, oriented along the radio axis (position angle 152°, PA1 in Table 1), giving a spectral resolution of 12 Å (FWHM).

Four separate exposures of 30 minutes each were taken on 21 March 1991. The seeing during the observations was $\sim 1.5''$. The conditions were photometric and the spectroscopic standard star EG54 was observed for flux calibration (Oke 1974). The raw spectra were flat-fielded, sky-subtracted, flux-calibrated and corrected for atmospheric extinction using the longslit package in the IRAF reduction package of the U.S. National Optical Astronomy Observatory. The accuracy of the wavelength calibration was $\sim$3 Å and we estimate that the flux calibration is good to $\sim$10%. A one-dimensional spectrum of 1243+036 was extracted using an aperture of 7″ to include all emission from the detected spatially extended emission line (see Sect. 3).

2.1.2. High resolution

High resolution optical spectroscopy of the Lyα emission line was carried out with EMMI on the ESO NTT on 14 April 1994. The detector was a Tektronix CCD having 2048^2 pixels with a scale along the slit of 0.27″ per pixel. The CCD was binned 2x2 giving an effective scale along the slit of 0.54″ per pixel. Using a 2.5″ wide slit with ESO grating 6, the spectral resolution was 2.8 Å. Four 1 hour exposures were taken with a slit orientation along the radio axis (152°, PA1), and one 1 hour exposure with the slit orientation angle orthogonal to the radio axis (at 62°, PA2). Conditions were photometric and the seeing was approximately 1″. The spectra were reduced in the same manner as the low resolution spectra described above. The [O I]λ 5577 Å

Table 1. The observations

Date	Telescope	Frequency/wavelength	Integration-time	Resolution
26 Nov 1988	VLA A-array	1465, 1515 MHz	300 s	$1''$
20 Aug 1991	VLA A-array	1465, 1515 MHz	2520 s	$1''$
20 Aug 1991	VLA A-array	8415, 8465 MHz	7200 s	$0.23''$
18 Mar 1994	VLA A-array	8085, 8335 MHz	1200 s	$0.23''$
18 Mar 1994	VLA A-array	4535, 4885 MHz	600 s	$0.43''$
01 Mar 1990	ESO 2.2 m	R band	2700 s	$1.0''$
21 Mar 1991	ESO NTT + EMMI	4100 to 7900 Å	7200 s (PA1)	$1.5'' \times 12$ Å
14 Apr 1994	ESO NTT + EMMI	5300 to 5900 Å	14400 s (PA1)	$1'' \times 2.8$ Å
14 Apr 1994	ESO NTT + EMMI	5300 to 5900 Å	3600 s (PA2)	$1'' \times 2.8$ Å
16 Apr 1994	ESO NTT + SUSI	5571 Å/60 Å	7200 s	$0.6''$
14 Jun 1994	UKIRT + CGS4	2.2 to 2.4 μm	3600 s	$1.5'' \times 0.006$ μm

Note: PA1 is slit position angle of 152° (along the radio axis), PA2 is 62°

skyline leaves strong residuals after sky subtraction and this region of the spectrum was therefore not taken into account in the analysis.

2.2. Radio

After the initial VLA "snapshot" observations described in Röttgering et al. (1994), further radio observations of 1243+036 were made on August 20, 1991 and March 18, 1994, using the VLA in 'A', configuration (see Table 1). The March 18, 1994 observations were part of a high resolution survey of a large sample of powerful radio galaxies at redshifts $z > 2$ (Carilli et al. 1996). All observations were made using a 50 MHz bandwidth.

Data processing was performed using the Astronomical Image Processing System (AIPS). The system gains were calibrated with respect to the standard sources 3C 48 and 3C 286. We estimate that the flux density scale is accurate to better than 1% at all frequencies. Phase calibration was performed using the nearby calibrator 1236+077. The (on-axis) antenna polarization response terms were determined, and corrected for, using multiple scans of the calibrator 0746+483 over a large range in parallactic angle. Absolute linear polarization position angles were measured using two scans of 3C 286 separated in time by a few hours. From the difference in solutions between these two we estimate the systematic uncertainty in the observed polarization position angles to be $\sim 1°$ at all frequencies.

The calibrated data were then edited and self-calibrated using standard procedures to improve image dynamic range. We have also combined the 1.5 GHz data presented in Röttgering et al. (1994) with the new data from August 20, 1991. The gridded visibilities were uniformly weighted to maximize spatial resolution. Images of the three Stokes polarization parameters, I, Q and U were synthesized, and all images were CLEANed down to the level of 2.5 times the theoretical RMS on the image, using the algorithm as implemented in the AIPS task MX. The observations at the different frequencies were added in the image plane, weighted by the root rms of the images, to produce the final maps at 8.3 GHz, 4.7 GHz and 1.5 GHz.

2.3. Narrow band imaging

Narrow band imaging was carried out with the ESO NTT using the Superb Seeing Imager (SUSI). A narrow band filter (ESO filter # 731) was used that has a central wavelength of 5571 Å and a bandpass width of 60 Å (FWHM). The detector was a Tektronix CCD with 1024^2 pixels and a scale of $0.12''$ per pixel. Four separate exposures of 30 minutes were taken each with a seeing better than $0.6''$. Each image was shifted by about $20''$ with respect to the previous to minimize problems due to flat-fielding and to facilitate cosmic ray removal. Image reduction was carried out using IRAF and AIPS. The individual images were bias-subtracted and flat-fielded using twilight exposures. The images were then registered using shifts determined from the peak positions of several stars on the CCD near the object and coadded after cosmic ray removal. To improve the signal to noise, the resulting image was smoothed with a Gaussian function having a full width half maximum of $0.37''$ (3 pixels) giving a final resolution, as measured from stars on the final image, of $0.6''$. Several stars that were visible on both the R-band image and the narrow band image were used to register the two images to an accuracy of $\sim 0.1''$. Absolute astrometric calibration was carried out using the Guide Star Catalogue (GSC) image processing system of the Space Telescope Science Institute (Lasker et al. 1990) resulting in an accuracy of $\sim 0.7''$.

2.4. Infrared

Infrared spectroscopy was performed on June 14, 1994, with the United Kingdom Infrared Telescope (UKIRT). The [O III] λ4959,5007 and Hβ λ4861 lines, redshifted into the K band window, were observed using the CGS4 spectrograph in the long camera mode, giving a pixel scale along the slit of $1.5''$ and a spectral resolution of 0.006 μm (~ 800 km s^{-1}). The object was observed in the beam-switching mode: the object was switched every 3 minutes between two different positions on the slit. The two series of observations were subtracted from each other to produce a sky-subtracted two-dimensional spectrum with a positive and a negative spectrum of the object. Further details of this observing method are described in Eales & Rawlings

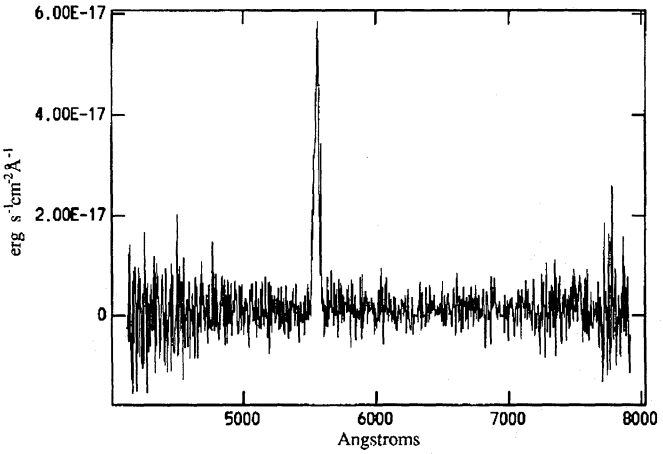

Fig. 1. The low resolution optical spectrum showing one bright emission line, identified with Lyα

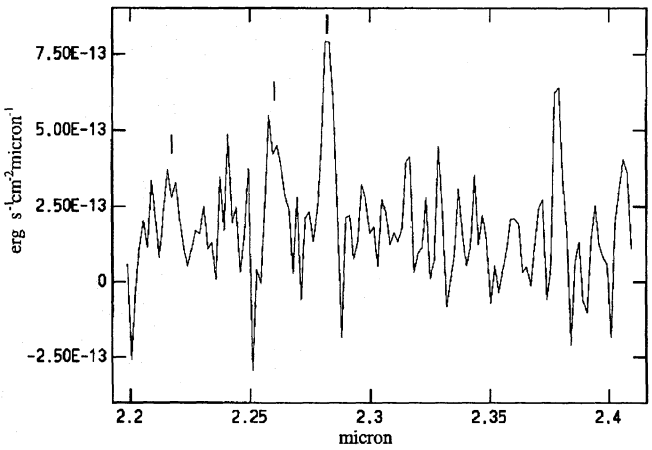

Fig. 2. The infrared spectrum showing the redshifted [O III] λ 5007 Å and 4959 Å emission lines and possibly Hβ (at 2.22 μm). The feature at 2.38 μm is not real, but due to a residual hot pixel on the array

(1993). The spectrum was extracted in a 7.5″ aperture (similar to that used for the optical low resolution spectroscopy) to include all extended line emission and wavelength and flux-calibrated using the "longslit" package as incorporated in IRAF.

A K-band image was obtained and reduced for us by Steve Eales and Steve Rawlings using IRCAM at the United Kingdom Infrared Telescope at Mauna Kea, Hawaii, in March 1993. It has a pixel scale of 0.62″ × 0.62″ and the total on source integration time was 1750 seconds. For more details on the IRCAM observations and reductions see Eales & Rawlings (1995).

3. Results

3.1. Low resolution spectroscopy: determination of the redshift

The low resolution optical spectrum showed one bright emission line (Fig. 1). This line is spatially extended by 7″, has an observed equivalent width of 1800 Å ±300 Å and an integrated flux of 2.7±0.3 × 10^{-15} erg s^{-1} cm^{-2} in the 7″ aperture. No further emission lines were seen in this spectrum. The faint continuum of 1243+036 is detected redward of the emission line. The continuum is not detected blueward of the emission line, giving a lower limit to the continuum drop of a factor 2.5 ±1. The large equivalent width of the line and the drop in continuum level at the emission line (similar to the continuum drop across the Lyα emission line in distant quasars due to intervening Lyα forest absorption, e.g. Steidel & Sargent 1987, and references therein) along with the faint R band identification and the small ultra steep spectrum radio source led us to tentatively identify the line with Lyman α at z = 3.57 ± 0.01. The redshifted Lyα line lies close to the strong [O I]λ5577 Å skyline making a more exact redshift determination difficult from the low resolution spectrum.

The infrared spectroscopic observation showed two bright emission lines in K band (Fig. 2). These were identified with the [O III]$\lambda\lambda$4959,5007 Å emission lines, indicating that the supposed redshift is indeed correct. There is also a hint of Hβ λ4861 Å emission. The [O III]5007 has a flux of 3 ± 0.5 × 10^{-15} erg s^{-1} cm^{-2}, comparable to that of Lyα, and has a spatial extent of at least 5″, i.e. comparable to the extent of Lyα in the low resolution optical spectrum. The spectrum of the emission lines in the infrared has much lower signal to noise ratio than that of Lyα in the optical. Therefore any faint [O III] emission in the region outside the radio lobes, if the [O III] would be equally extended as the Lyα (see below), could not be detected.

3.2. Radio polarimetric imaging

Figure 3a shows the total intensity image at 8.3 GHz with 0.23″ resolution, Fig. 3b shows the image at 4.7 GHz with a resolution of 0.43″ and Fig. 4 shows an image at 1.5 GHz with 1″ resolution, produced from the combined data from Röttgering et al. (1994), and later observations at the same frequency. A number of features have been labeled for reference. Table 2 lists the positions of the peaks, the peak surface brightnesses (I) and integrated fluxes (S, measured in a rectangular box around the components) for the various source components.

The detailed source structure is best represented in the 8.3 GHz image (Fig. 3a). The northern lobe (designated 'A') has a compact component with a 'tail' extending to the north. The southern lobe (designated 'B') again has a compact component (B1) close to the nucleus, and a linear series of knots (the southern 'jet'), extending towards the south from B1, with a slight extension to the west at its southern end. In between these two lobes is a faint region of emission (designated 'N'), that has a core–jet structure with a length of about 0.8″, oriented in a position angle of −24°, i.e. roughly aligned with the axis defined by components A1, N, and B1. The southern jet lies at an angle of 30° away from this axis.

The spectral index image of the 8.3 GHz and 4.7 GHz maps convolved to 0.43″ resolution (with a cut-off where the signal to noise ratio in the original maps is smaller than 8) is shown in Fig. 5a, and of the 4.7 GHz and 1.46 GHz maps convolved to 1″ resolution is shown in Fig. 5b. Spectral index values between 8.3 GHz and 4.7 GHz, determined from the surface

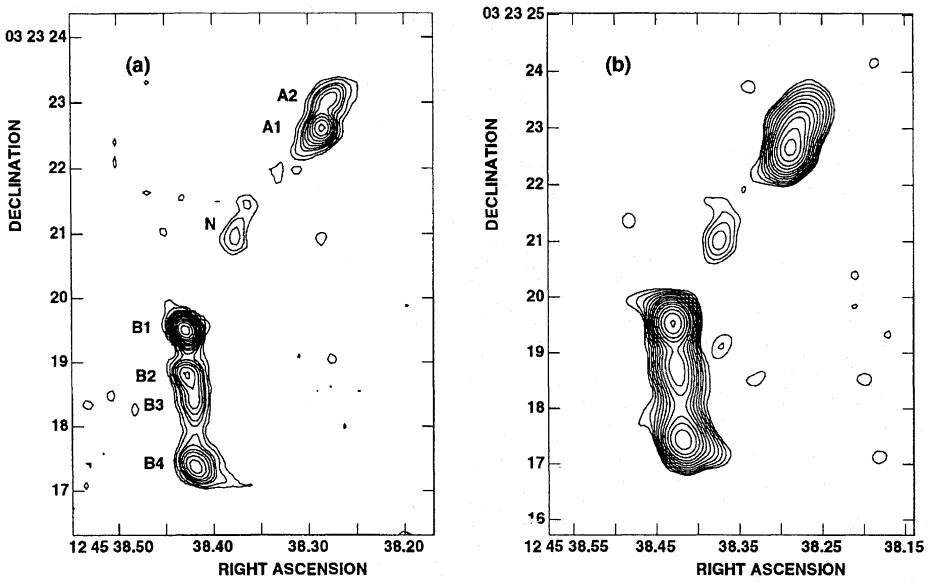

Fig. 3. a An image of 1243+036 at 8.3 GHz with a Gaussian restoring beam of FWHM = 0.23″. The contour levels are a geometric progression in $2^{1/2}$. The first contour level is 0.13 mJy, which is three times the off-source RMS in the image. **b** An image of 1243+036 at 4.7 GHz with a Gaussian restoring beam of FWHM = 0.43″. The contour levels are a geometric progression in $2^{1/2}$. The first contour level is 0.2 mJy, which is three times the off-source RMS in the image

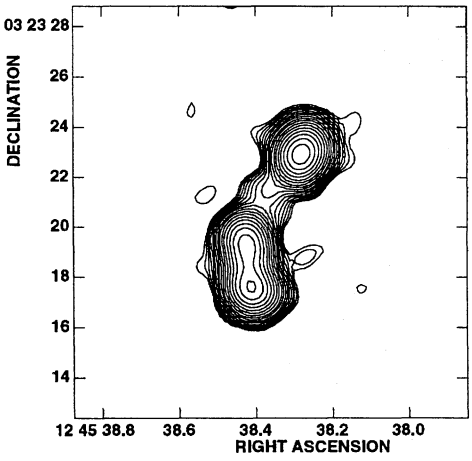

Fig. 4. An image of 1243+036 at 1.46 GHz with a Gaussian restoring beam of FWHM = 1″. The contour levels are a geometric progression in $2^{1/2}$. The first contour level is 0.3 mJy, which is three times the off-source RMS in the image

brightness of the various source components convolved to the same resolution, are also listed in Table 2. Most components of the radio source have steep spectra, with indices typically < -1.4. The two exceptions are components B1 and N, both of which have flatter spectral indices of ~ -1.0. One curious aspect of the 1243+036 radio structure is that the spectral index distribution steepens with distance from the source centre in both components A and B. This is unlike most high power radio galaxies, which show the flattest spectral indices at the radio hot spots situated at the extremities of the radio source (Carilli et al. 1991, Alexander & Leahy 1987). This spectral steepening may be due to synchrotron radiation losses of the highest energy electrons.

We assume minimum energy conditions (see Miley 1980; Pacholczyk 1970) to derive a minimum magnetic field strength. In calculating the minimum energies we assume that the radio source is cylindrically symmetric, the plasma has unit filling factor and that the synchrotron spectrum extends from 10^7 to 10^{11} GHz. For the components with high frequency spectral index $\alpha_{8.3}^{4.7} < -1.0$ a two–slope power-law spectrum was assumed with a spectral index below 4.7 GHz (observed frame) of -1.3, equal to the integrated source spectral index between 178 MHz and 2700 MHz. The derived parameters for the various components are in Table 3.

We can estimate the density of the external medium assuming that the minimum pressures are balanced by either ram pressure, due to the propagation of the radio plasma at a velocity of a few thousand km s^{-1} (e.g. Cygnus A, Carilli et al. 1991 and references therein), or by thermal pressure from a hot ($\sim 10^7$ K) external medium, which is often found to be present around powerful radio galaxies and in clusters at low redshifts (see Crawford et al. 1988; Baum et al. 1989 and references therein). For the typical source parameters, we find that the external density ranges from 0.1 cm^{-1} (ram pressure) to several tens of cm^{-1} (thermal pressure), see Table 4.

Assuming that the spectral steepening of the outer components relative to the inner components is due to synchrotron radiation losses, we crudely estimate the synchrotron age of the emitting radio plasma in a few components from the break frequency where the radio spectrum steepens and the magnetic field strength. We estimate the restframe break frequency by fitting a "Kardashev-Pacholczyk model" to the spectral index distribution in Figs. 5a and 5b and assuming that the input spectral index $\alpha_{in} = -0.7$ (spectral index at frequencies below the synchrotron break). For more details about spectral ageing modelling see Carilli et al. (1991). The synchrotron age of the radio plasma is given by: $t_s = 1610 B^{-3/2} \nu_B^{-1/2}$ Myr with B in μG and ν_B in GHz, see Carilli et al. (1991). We note however that there are large uncertainties in these ages, because of the strong dependence on the magnetic fields that are derived from the high restframe frequencies only. In any case, the derived synchrotron

Table 2. Results from the radio polarimetric imaging of 1243+036

Comp.	$I_{8.3}$ (mJy/beam)	$I_{4.7}$ (mJy/beam	$S_{8.3}$ (mJy)	$S_{4.7}$ mJy	R.A. (J2000)	Decl. (J2000)	α	$FPol_{8.3}$ (%)	$D_{8.3}^{4.7}$
A2	0.95		2.1		$12^h45^m38.28^s$	03° 23′ 23.1″			
A1	3.25	10.62	5.2	20.3	38.29^s	22.6″	−1.7	4.4	<0.30±0.1
N	0.31	0.70	0.7	1.4	38.37^s	21.0″	−1.0		
B1	9.87	19.19	11.8	22.2	38.43^s	19.5″	−1.0	<2.0	
B2	1.49	5.91	2.8	11.6	38.43^s	18.8″	−1.6	17	0.55±0.1
B3	0.93		1.8		38.42^s	18.4″			
B4	1.80	8.56	3.8	14.1	38.42^s	17.4″	−2.0	0.30	1.3±0.5

Notes: (1) I is the peak surface brightness. S is the integrated flux measured in a rectangular box around the component. α is the spectral index between 4.7 GHz and 8.3 GHz determined from the surface brightness after concolving the maps to the same resolution. $FPol_{8.3}$ is the fractional polarization at 8.3 GHz and $D_{8.3}^{4.7}$ is the depolarization of the radio emission between 4.7 and 8.3 GHz. (2) The components A1, A2 and components B2, B3 are unresolved at 4.7 GHz. Values at this frequency stated only for A1 and B2 are actually for A1+A2 and B2+B3.

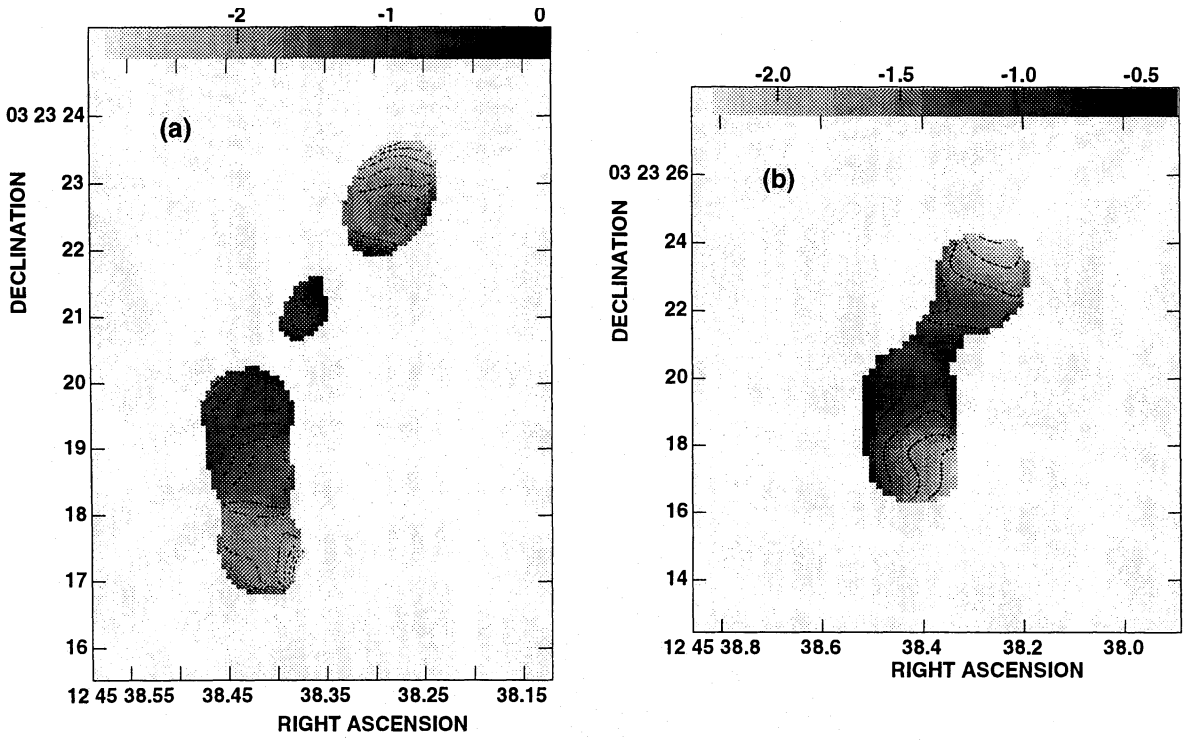

Fig. 5. a An image of the spectral index distribution of the radio emission from 1243+036 at 0.43″ resolution between 8.3 GHz and 4.7 GHz. The contour levels are: -2.8, -2.4, -2.2, -2.0, -1.8, -1.6, -1.4, -1.2, -1.0, -0.8, -0.4 and -0.2. The grey-scale ranges from -3 (white) to -0.3 (black). **b** An image of the spectral index distribution of the radio emission from 1243+036 at 1″ resolution between 1.46 GHz and 4.7 GHz. The contour levels are: -2.2, -1.9, -1.6, -1.3, -0.9, -0.6, -0.3 and 0.0. The grey-scale ranges from -2.3 (white) to -0.3 (black)

ages give an impression of the age of the outer components (B4) relative to the inner components (B1). The derived synchrotron ages for the components A1, B1 and B4 are listed in Table 3.

Images of polarized intensity from 1243+036 are shown in Fig. 6, along with vectors representing the position angle of the electric field vectors. The only component that shows substantial polarization at both frequencies is the southern jet (components B2, B3, and B4). Component A shows weak polarization at 8.3 GHz, and no polarized emission at 4.7 GHz, and components B1 and N show no polarized emission at either frequency. The fractional polarization of these various components (4σ upper limit for B1) are listed in Table 2. Also listed are the depolarization ratios, $D_{8.3}^{4.7}$, for the components with detected polarized signal, where $D_{8.3}^{4.7}$ is the ratio of fractional polarization at 4.7 GHz to that at 8.3 GHz. Component B4 shows no significant depolarization between 4.7 GHz and 8.3 GHz, while component B2 has a value of $D_{8.3}^{4.7} = 0.55$, and A1 only has an upper limit (4σ) of $D_{8.3}^{4.7} < 0.3$.

We estimate that the uncertainties in observed position angle in the brighter polarized regions are about 2°, based on

Table 3. Physical parameters from the radio emission of 1243+036

Comp.	$P_{4.7\,GHz}$ ($\times 10^{27}$ W Hz^{-1})	L_{tot} ($\times 10^{45}$ erg s^{-1})	B_{min} ($\times 10^{-4}$ Gauss)	E_{min} ($\times 10^{-9}$ erg cm^{-3})	Minimum total energy (10^{58} erg)	P_{min} ($\times 10^{-9}$ dyne cm^{-2})	ν_{break} (GHz)	t_{synchr} (10^3 yr)
Integrated	11	7.1						
A2			24	540	13.7	180		
A1	2.2	1.7	11	116	3.0	39	~ 24	~ 5
N	0.07	0.06	3	9	0.2	3		
B1	1.9	0.9	8	62	0.7	21	~ 120	~ 5
B2	0.9	1.0	16	227	2.6	76		
B3			14	173	2.0	58		
B4[a]	1.5	1.2	11	112	1.3	37	~ 25	~ 10

[a] Minimum energy requirements for B4 were derived using the overall spectral index -1.3, because the high frequency spectral index -2.0 would greatly overestimate its total luminosity.

Notes: (1) The components A1, A2 and components B2, B3 are unresolved at 4.7 GHz. Values at this frequency stated only for A1 and B2 are actually for A1+A2 and B2+B3. (2) For calculation of the luminosity of the components with high frequency spectrum steeper than -1.0, a two-slope power law spectrum was assumed with a spectral index below 4.7 GHz (observed frame) of -1.3, equal to the integrated source spectral index.

Table 4. Density of the external medium from confinement by Ram pressure and static thermal pressure

Component	$(n_e)_{ext}$	
	Ram $v = 3 \times 10^3$ km s^{-1} (cm^{-3})	$T = 10^7$ K (cm^{-3})
A2	1.2	56
A1	0.3	12
N	0.02	1.0
B1	0.1	6.6
B2	0.5	24
B3	0.4	18
B4	0.3	12

signal-to-noise and possible systematic errors of $\sim 1°$ discussed in Sect. 2. Overall, we feel that a position angle change of $\geq 6°$ between 8.3 GHz and 4.7 GHz could have been measured with this data at the peaks in polarized intensity. No such change is seen, implying an upper limit to the rest frame rotation measures of $\sim$1000 rad m^{-2}. This limit applies to the regions that are not depolarized.

The projected magnetic field distribution is shown in Fig. 7 overlaid on the 8.3 GHz total intensity map. In the southern region, the projected field is parallel to the jet, and then bends towards the west in the vicinity of knot B4. In the north the projected field is parallel to the 'tail' of component A towards the northwest. Towards the west of knot B4 there is slightly extended radio emission visible at all three radio frequencies. This emission and the change of the magnetic field direction at that position suggest that this may be outflow from the final hotspot (B4) into the radio lobe.

3.3. Optical and IR imaging

3.3.1. Broad band imaging

The R band image identifying the radio source is from Röttgering et al. (1995b). The optical identification is a faint 2″–3″ extended galaxy with an integrated magnitude of R = 22.5 (Röttgering et al. 1995b). In the low resolution optical spectrum, continuum emission is detected but no emission lines were detected in the R band region of the spectrum. The strongest emission line that might affect the R band flux is C IVλ1549 Å (expected at 7079 Å) but was not detected, so that the R band does not contain any appreciable contribution (less than 5%) from line emission. The R band image therefore represents the continuum emission from 1243+036. The optical galaxy is clearly aligned with the main radio axis, as is common in high redshift radio galaxies (Chambers et al. 1987, McCarthy et al. 1987). In Fig. 8 the same R band image is rebinned and smoothed with a Gaussian of FWHM 1.0″ and overlaid with the contours of the 8 GHz VLA map. There appears to be faint extended continuum emission in the direction of the principal radio axis that extends beyond the radio lobes (indicated A and B in Fig. 8). Although at a low surface brightness, the total extended emission is detected at a signal to noise of $\sim$10 in both north (A) and south (B). Three more small blobs at the 10σ significance level are seen on the smoothed frame (indicated C, D and E) in the region to the southwest of 1243+036, while elsewhere on the CCD frame such a concentration of emission features is not observed.

The K-band image obtained at UKIRT gave a magnitude for 1243+036 in a 5″ aperture of K=18.8 $\pm$ 0.2. However, the K-band flux includes the strong redshifted [O III] emission line (see Fig. 2). After correcting for the [O III] flux as determined from the infrared spectroscopy, we find a continuum K magnitude of 19.3 $\pm$ 0.3. This K-band magnitude is typical for radio galaxies at these redshifts (e.g. Eales & Rawlings 1993; Eales

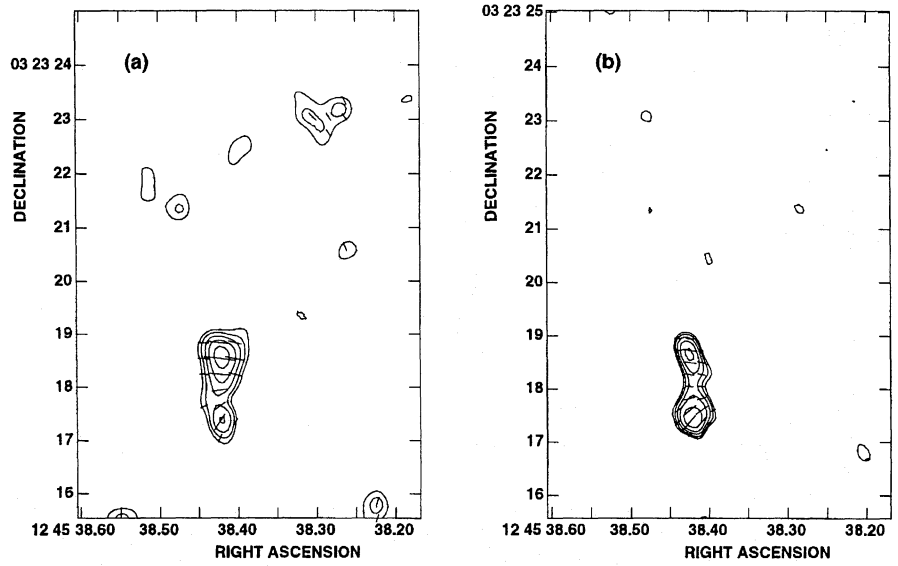

Fig. 6. a An image of linear polarized intensity from 1243+036 at 8.3 GHz with a resolution of 0.43″. The contour levels are a geometric progression in $2^{1/2}$. The first contour level is 0.11 mJy. The line segments show the orientation of the electric vectors for the polarized emission. **b** An image of linear polarized intensity from 1243+036 at 4.7 GHz with a resolution of 0.43″. The contour levels are a geometric progression in $2^{1/2}$. The first contour level is 0.18 mJy. The line segments show the orientation of the electric vectors for the polarized emission

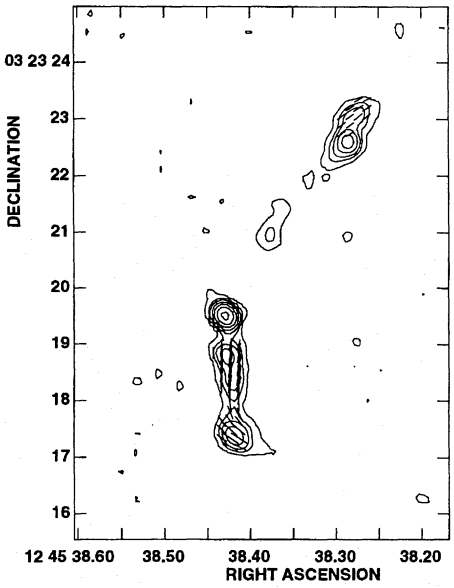

Fig. 7. The contours show the total intensity radio emission from 1243+036 at 8.3 GHz. Contours are at 0.03 mJy x (-4, 2, 8, 16, 32, 64, 256, 512). The line segments show the orientation of the projected magnetic field vectors, derived from the polarized emission

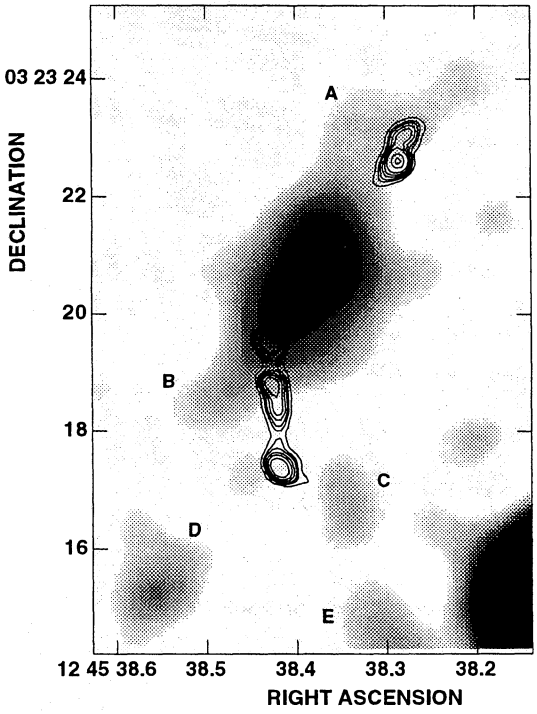

Fig. 8. Smoothed R band image from Röttgering et al. (1995b) with the contours of the 8.3 GHz radio image overlayed

et al. 1993b). The signal to noise ratio of the detection was low and the image is therefore not shown. A Keck-telescope image in K band shows that it is aligned with the optical and radio structure (van Breugel, private communication).

3.3.2. Narrow band Lyman α imaging

A contour image of the Lyman α emission from 1243+036 is shown in Fig. 9. The peak, measured as the position of the maximum of a two-dimensional parabolic fit to the brightness distribution, is at $12^h45^m38.36^s$, $03^o\ 23'\ 21.1''$. The Lyα emission has a complex morphology: (1) 'Cone-shaped' emission extends along the radio axis towards the south–east for about 2″. (2) On a scale of $\sim$ 5″ the gas shows two 'arms' of emission both extending almost due south, originating from the southern end of the inner cone of emission. (3) To the north there is faint emission which extends about 3″ from the Lyα peak at a position angle of about $-25°$. (4) The lowest surface brightness Lyα emission on scales of 8″ has a clumpy or filamentary structure. This clumpy structure is at a level of 4–6σ. (5) There is a small region of enhanced line emission at the southern end

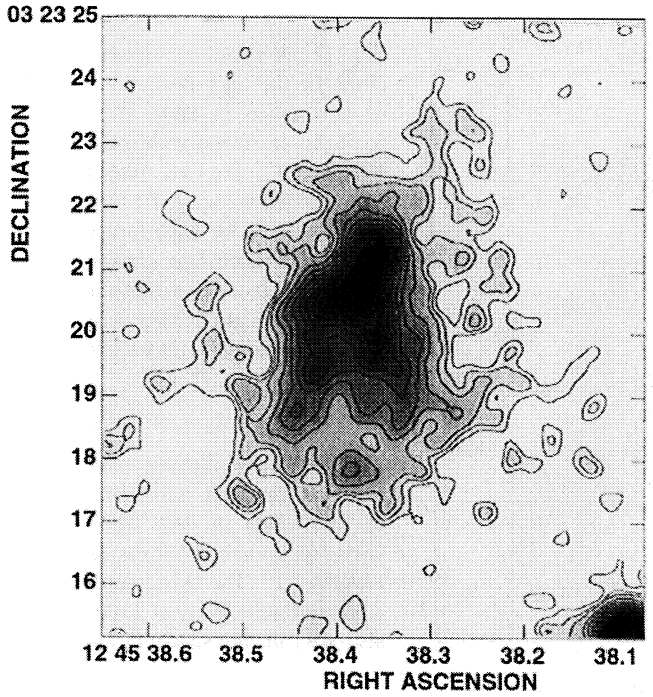

Fig. 9. Image of the Lyα emission associated with 1243+036 with a resolution of 0.6″. Contours linearly spaced are at $2\sigma, 4\sigma, 6\sigma$,..., where σ is the background rms noise

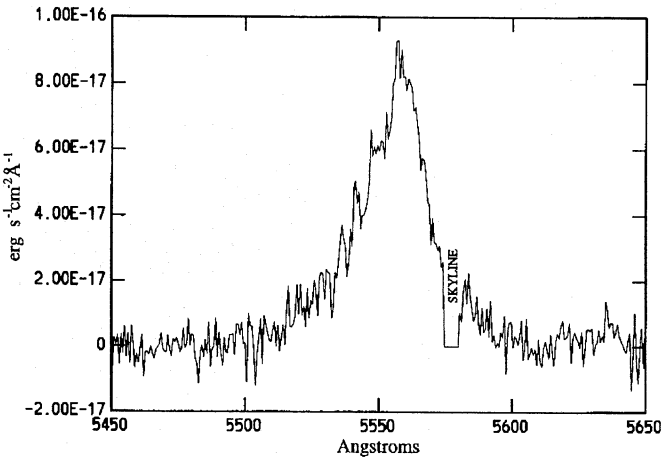

Fig. 10. The spectral profile of the central Lyα emission at high resolution (2.8 Å) in position angle along the radio axis (PA1). Details on the profile are described in the text

of the Lyα emission, due south of the 'gap' between the two 'arms', mentioned above.

3.4. High resolution spectroscopy

The positions of the slits used in the 2.8 Å resolution spectroscopy are shown in Fig. 14. The spectrum with the slit along the radio axis (PA1=152°) shows the velocity field of the central and most spatially extended Lyα. The overall shape of the central velocity profile (Fig. 10) has a width of $\sim 1550 \pm 75$ km s^{-1} (FWHM). The line does however not have a smooth shape. It has several small dips (or peaks), especially in the blue wing of the Lyα emission line. These small dips at 5533, 5538, 5544 and 5550 Å were present in the individual exposures.

The two-dimensional Lyα spectrum in PA1, smoothed with a Gaussian of FWHM 2 pixels (1.1″) to enhance fainter extended Lyα emission, is shown in Fig. 11. Most of the flux is in the centre and has a spatial extent of $\sim 2''$ that peaks at 5557 Å,i.e. $z = 3.5699 \pm 0.0003$. The total flux of Lyα is better determined from the high resolution spectrum, since the subtraction of the skyline at 5577 Å can be carried out with a much greater accuracy than in the low resolution spectrum. The integrated Lyα flux in an aperture of 11″ is $2.9 \pm 0.2 \times 10^{-15}$ erg s^{-1} cm^{-2} corresponding to a luminosity of $\sim 2.7 \times 10^{44}$ erg s^{-1}. In a larger aperture of 24″, including the most extended emission seen in the smoothed two-dimensional spectrum (see below and Fig. 11), the Lyα flux is 3.2×10^{-15} erg s^{-1} cm^{-2}.

A separate velocity component in Lyα emission is seen at about 1100 km s^{-1} blueward and 2″ southward along the slit from the central Lyα peak. This component contains almost 10% of the total Lyα flux and has a velocity width of $\sim 1200 \pm 100$ km s^{-1} (FWHM). Its position coincides with the brighter of the two 'arms' of Lyα emission seen in the Lyα narrow band image and with radio component B1 (see below).

There is also a remarkable, extended narrow component (~ 250 km s^{-1} FWHM) that clearly shows a velocity shear on both sides of the nucleus. It has a total spatial extent of $\sim 20''$, corresponding to 136 kpc, much larger than the size of the radio source (8″). The velocity difference between the northern and southern extent of this emission is ~ 450 km s^{-1}.

Note that this very extended Lyα component was not seen in the narrow band Lyα image. This is because the resolution of the spectrum is very well matched to the velocity width of the most extended Lyα gas, whereas the narrow band filter has a much larger spectral width. Also the presence of the 5577 Å skyline adds a considerable amount of noise in the narrow band image.

The small dips seen in the one-dimensional spectrum are also clearly visible on the two-dimensional spectrum (Fig. 11). Especially noteworthy is the feature at $\sim$ 5533Å, that extends spatially from the central Lyα emission to the separate velocity component at B1.

The high resolution spectrum taken with the slit perpendicular to the radio axis (PA2=62°, Figs. 12 and 13) shows only the Lyα emission from the brightest inner part as seen on the Lyα narrow band image. The emission is spatially resolved. The emission has the same overall velocity width and peaks at the same wavelength as the spectrum taken along the radio axis. The two-dimensional spectrum shows a depression in the Lyα emission blueward of the peak in the central rows of the spectrum over about 6 Å (~ 300 km s^{-1}). The Lyα emission blueward of the depression has the same velocity as that of the separate velocity component described above along PA1. Redward of the depression the Lyα has the same velocity as that of the brightest inner Lyα in the PA1 spectrum. The signal of the main Lyα

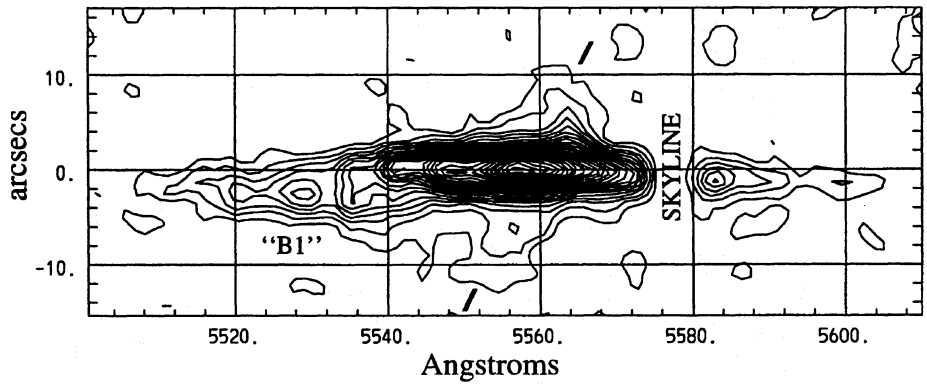

Fig. 11. A two-dimensional representation of the high resolution spectrum of Lyα taken in PA1. The spectrum has been smoothed with a Gaussian of FWHM 1.1″. The Lyα component with a blueshifted velocity of 1100 km s^{-1} is marked "B1". We have further marked the narrow width Lyα emission with a velocity shear and an extent of more than 20". Contours are linearly spaced at 2σ, 4σ, 6σ,..., where σ is the background rms noise

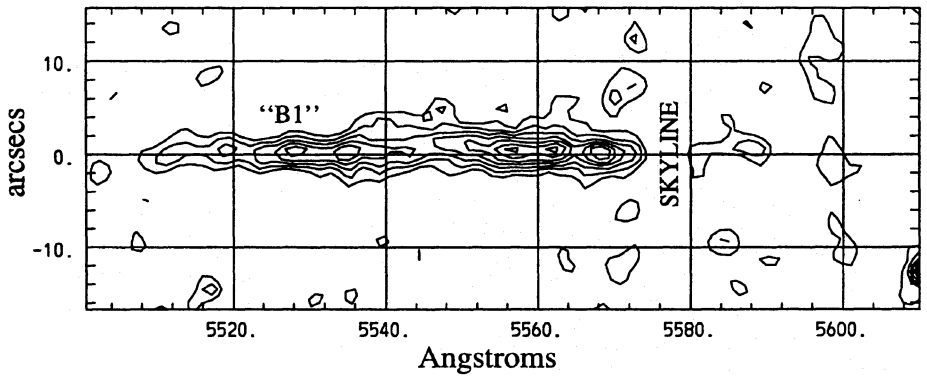

Fig. 12. A two-dimensional representation of the high resolution spectrum of Lyα taken in PA2. The spectrum has been smoothed with a Gaussian of FWHM 1.1″. The Lyα component with a blueshifted velocity of 1100 km s^{-1} is also seen in this spectrum and marked "B1". Very extended Lyα emission with a velocity shear and narrow width as seen in the spectrum along the radio axis is not seen along PA2. Contours are linearly spaced at 2σ, 3.5σ, 5σ,..., where σ is the background rms noise

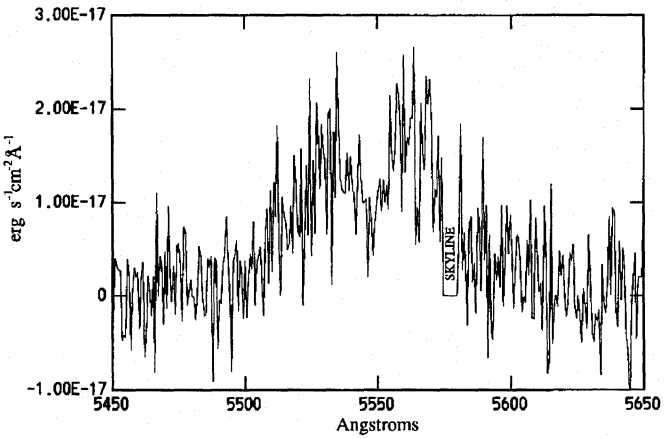

Fig. 13. The spectral profile of the central Lyα emission at high resolution (2.8 Å) in position angle perpendicular to the radio axis (PA2). The slit was positioned slightly off the brightest central Lyα emission, therefore including emission from component B1 (5530 Å)

emission is not as strong as in the PA1 spectrum. Therefore it seems that the 2.5″ wide slit was not exactly positioned at the peak of Lyα and the blueshifted Lyα emission at the position of B1 is also at least partly included (see Fig. 14).

The very extended low surface brightness Lyα seen in the spectrum along the radio axis (PA1) is not seen in the spectrum with the perpendicular slit position (PA2). Although the spectrum at PA2 is not as deep as that at PA1 (the noise is a factor 2 higher), such faint emission would have been detected if it was of the same extent and surface brightness as the emission observed along the radio axis.

3.5. Description of the various components

Figure 14 shows the Lyman α image of 1243+036 overlaid with the radio continuum emission at 8.3 GHz. Figure 8 shows the same radio image overlaid with the R band optical image. Standard VLA astrometry is accurate to at least 0.2″, the optical astrometry has an accuracy of 0.7″ (Röttgering et al. 1995b) so that the uncertainty in the registration of the optical and radio images is of the order of 1″.

The spatial extent of the Lyα emission visible in the narrow band image is similar to that of the radio source (~8″). Component N of the radio source is located at the peak of the line emission and R-band emission. Since N is also the flattest spectrum radio component, we identify it as the centre of the nuclear activity of 1243+036. The spatial extent of this radio core–jet component (length $\approx$ 0.8″) is comparable to the spatial extent of the highest surface brightness line emission.

The radio galaxy 1243+036 exhibits two trends seen in samples of high redshift radio galaxies (*cf.* McCarthy 1993a). Firstly, the alignment between the major axis of the line emitting gas and the optical continuum with the principal axis of the radio source. Secondly, the emission line gas is distributed asymmetrically with respect to the nucleus. In most powerful radio galaxies the emission line gas is brightest on the side of the clos-

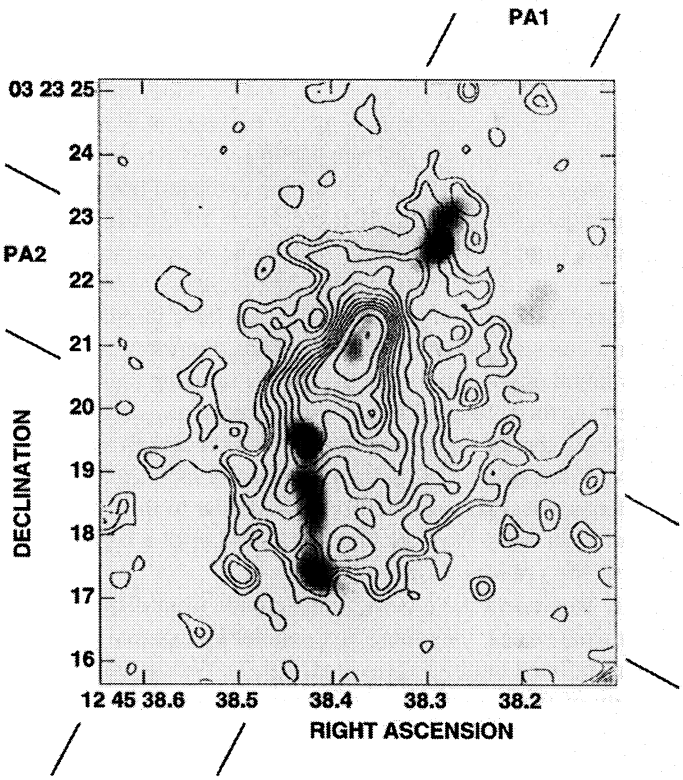

Fig. 14. The Lyα image of 1243+036 in contours with the 8.3 GHz VLa map in greyscale superimposed. Radio component B1, the bending point of the radio structure, coincides with enhanced Lyα emission in one of the 'arms'. Indicated around the edges are the slit positions, PA1 and PA2, that were used in the high resolution spectroscopy

est radio lobe, suggesting interaction between the radio source and the ambient gaseous medium (McCarthy et al. 1991). Regarding the entire extent of the radio lobes of 1243+036, the southern radio lobe (B) is not the closest to the nucleus (N). However, regarding the brightest hotspots in the lobes, A1 and B1, B1 is the closer with an armlength ratio of Q=1.2. Further, the southern lobe is the most distorted and brightest, indicating a stronger interaction with the environment.

In addition to these two trends, there are three further correlations in the radio and Lyα properties. Firstly, both the line emitting gas and the radio source show peculiar structure at the position of component B1. The radio source bends by about 30° towards the south. The line gas has a local peak at this position, and the long slit spectra show that the line emitting gas in this region is blueshifted by $\sim$ 1100 km s^{-1} with respect to the central ionized gas. The southern jet follows closely along the brighter of the two southern 'arms' of line emission. Secondly, the emission line gas is seen to encompass the northern radio source component A. The high resolution spectrum (Fig. 11) shows that the Lyα has a low surface brightness component that extends far beyond the radio lobes. Thirdly, the emission line gas inside the radio structure is brighter and has a much larger velocity dispersion than the emission line gas outside the radio structure.

Summarizing the results from the high resolution spectroscopy and narrow band imaging of the Lyα gas we can distinguish between three separate components of the emission line gas:

3.5.1. The high velocity dispersion gas inside the radio structure, the *"inner halo"*

The Lyα emission within a radius defined by the maximum extent of the radio structure is dominated by the bright central emission which has the shape of a cone with a large velocity dispersion ($\sim$ 1550 km s^{-1} FWHM). Such a velocity dispersion is typical for the extended emission line gas in high redshift radio galaxies (McCarthy 1993, McCarthy 1989).

3.5.2. Enhanced Lyα emission with a blueshifted velocity at the position of radio knot B1

The region of enhanced Lyα emission at the position of radio knot B1, in the brighter of the two southern arms, has a clear velocity difference ($\sim$ 1100 km s^{-1}) relative to the central Lyα. Its velocity dispersion ($\sim$ 1200 km s^{-1} FWHM) is similar to the rest of the Lyα gas in the inner halo.

3.5.3. Lyα emission extended far beyond the radio source, the *"outer halo"*

The very extended Lyα emission with a velocity shear of $\sim$ 450 km s^{-1} has a total spatial extent of $\sim$ 20″ (136 kpc), much larger than the radio source ($\sim$ 8″). This indicates that this component of the gas has no direct relation with the radio plasma. This extended Lyα was seen with the slit of the spectrograph along the principal radio axis. The spectrum perpendicular to the radio axis showed that in this direction there is no Lyα emission of such extent.

4. Discussion

4.1. Ionization, density and confinement of the Lyα emitting clouds and density of the external medium

Several mechanisms have been considered for the ionization of the extended emission line clouds in powerful radio galaxies. These include ionization by UV radiation from hot stars, shock ionization from the interaction with the radio lobes and photoionization by the active nucleus. The equivalent width of the Lyα emission in most high redshift radio galaxies is several times larger than can be produced by hot stars (McCarthy 1993, Charlot & Fall 1993). In general, the line ratios in radio galaxies are not well reproduced by shock ionization nor ionization by hot stars and indicate that photoionization by nuclear UV radiation appears to be the dominant mechanism of ionization (Baum & Heckman 1989, Baum et al. 1992, McCarthy 1993, Ferland & Osterbrock 1986, Ferland & Osterbrock 1987). Anisotropic photoionization by an obscured nucleus has been argued to explain the deficit of observed

UV photons from radio galaxies and Seyfert-2 galaxies relative to the amount needed to produce the emission line luminosities (Antonucci & Miller 1985). This concept has been an important constituent of orientation-based unification models of radio galaxies and quasars, which can explain many observed correlations and anomalies (Scheuer 1987, Barthel 1989, Hes et al. 1993). In these models radio-loud quasars and radio galaxies are intrinsically similar objects but observed at different angles. The radiation from the nucleus escapes preferentially within a cone along the radio axis and ionizes the gas clouds in its path. In quasars we can see inside the ionizing cone and see the broad-line emission region close to the active nucleus, while in radio galaxies the nucleus is obscured so that we cannot see the ionizing radiation directly, but see the extended (narrow) emission line region that is ionized by the nuclear continuum. The alignment of the ionized gas with the radio axis in most powerful radio galaxies argues in favour of these models, especially the presence of ionized gas outside the radio lobes. The Lyα emission in the outer halo in 1243+036, outside the radio lobes, but aligned with the principal radio axis, rules out shock ionization by the radio source and strongly argues for photoionization by anisotropic nuclear emission. 4C 41.17 at z = 3.8 (Chambers et al. 1990) and 6C 1232+39 at z = 3.2 (Eales et al. 1993a) are other examples of high redshift radio galaxies with Lyα emission extending beyond the extent of the radio emission. The "cone" shaped morphology of the innermost 2″ of the Lyα emission of 1243+036 would not be expected from shock ionization and further supports the idea that the Lyα halo of 1243+036 is indeed photoionized by anisotropic nuclear continuum radiation. The shape of this innermost Lyα emission region indicates an opening angle for the cone of nuclear ionizing radiation of between 35° and 50°.

Although we have very little information on the physical conditions of the ionized gas we can estimate the density and mass of the emission line gas, assuming photoionization, from the flux and extent of the Lyα emission along the lines of McCarthy et al. (1990) for 3C 294 and Chambers et al. (1990) for 4C 41.17. We shall use three different approaches to estimate the density.

I. Following McCarthy (1990), the Lyα luminosity is related to the density of the ionized gas, assuming case B recombination: $L = 4 \times 10^{-24} n_e^2 f_v V$ erg s^{-1}, where V is the total volume occupied by the emission line gas and f_v the volume filling factor of the gas. From this then follows the mass in ionized gas M$\approx n_e m_{\rm proton} f_v V$. Because we have no means of measuring the filling factor and density simultaneously in 1243+036, we have to estimate the volume filling factor. From direct measurements, using sulphur lines, of the density of line emitting gas in low redshift radio galaxies, filling factors in the range 10^{-4}–10^{-6} and typically of order $\sim 10^{-5}$ have been found (van Breugel et al. 1985, Heckman et al. 1982). Assuming a filling factor $f_v \sim 10^{-5}$ we give in Table 5 the density of several components of the Lyα halo and their inferred masses. The sizes of components were measured from the Lyα image and high resolution spectroscopy and were assumed to be cylindrically symmetric. The values derived in Table 5 indicate that the density of the ionized gas falls off with radius as r^{-2}. This would mean that in the case of anisotropic nuclear photoionization the ionization parameter would be about the same at all radii. This is consistent with the findings of Baum et al. (1992) for the emission line nebulae in powerful radio galaxies at low redshifts and also found for the extended line emission around quasars at $z > 0.5$ (see Bremer et al. 1992 and references therein). The Lyα peak at B1 seems to be an exception. However, as we will argue in Sect. 4.3, the jet–gas interaction that bends the radio jet at the position B1, may have shredded dense neutral cores of the emission line clouds, therefore increasing the amount of gas exposed to the nuclear ionizing radiation and increasing the volume filling factor of ionized gas, consequently enhancing the Lyα emission at that position (see Bremer et al. 1996). If the volume filling factor is locally increased to 10^{-3}, the density decreases to $\sim$100 cm^{-3}, similar to that in the rest of the inner halo. We note that this would infer a higher mass ($\sim 10^8$ M$_\odot$) of ionized gas at B1.

II. To prevent the emission line clouds from dispersing on short time scales, they must be confined by external pressure, as was pointed out by Fabian et al. (1987). We can estimate the density of the emission line filaments, assuming that they are confined by a hot ($\sim 10^7$ K) external medium, with density derived from the radio data. The emission line clouds may also be confined by the pressure from the radio lobes, however the radio lobes in turn must be confined by an external medium, leading to the same pressure requirement. Further evidence for the presence of a hot halo comes from the strong depolarization of the radio emission, that is most likely caused by a hot (X-ray) halo as magnetoionic medium (Laing 1988a, Garrington et al. 1988). Other HZRGs (e.g. 4C 41.17 and B2 0902+34, Carilli et al. 1994) show evidence for the presence of a hot surrounding halo. Unfortunately, at the high restframe frequencies observed, the radio emission from the extended lobes is not detected and the emission is dominated by the emission from the hotspots. The hotspots are most likely confined by the ram pressure caused by their propagation through the external medium and not by static thermal pressure. Because of its flatter radio spectrum hot spot B1 appears to be the most "active" and we therefore assume the balance between minimum pressure and ram pressure from B1 to be the best representative pressure. Ram pressure confinement of the advancing hotspot requires a density of $\sim$0.1 cm^{-3} (see Table 4 and Sect. 4.3). Hotspot A1 requires a similar density. Assuming pressure balance between the hot halo gas ($nT \sim 10^6$ K cm^{-3}) and the emission line clouds (with a temperature of $\sim 10^4$ K) gives an average density of the ionized gas of $\sim$100 cm^{-3}, roughly consistent with the emission line gas density derived assuming $f_v \sim 10^{-5}$.

III. Assuming that every ionized hydrogen atom eventually results in the emission of a Lyα photon, the Lyα luminosity indicates the necessary flux of ionizing photons, $Q_{\rm ion} \approx 2\times10^{55}$ photons s^{-1}. Using this and an estimate of the ionization parameter, U, of the gas gives a third estimate of the density: $U=Q_{\rm ion}/4\pi r^2 n_e c$. In 1243+036 we have no emission lines from which we could directly estimate the ionization parameter. However, from photoionization modelling of high and low redshift

Table 5. Density and mass of the ionized gas assuming $f_v = 10^{-5}$

Lyα Component	Size (kpc^3)	$L_{Ly\alpha}$ (10^{44} erg s^{-1})	(n_e) (cm^{-3})	Mass (10^8 M$_\odot$)
Inner halo	$55 \times 27 \times 27$	2.7	80	7
Central peak	$14 \times 6 \times 6$	1	400	0.4
Peak at B1	$4 \times 4 \times 4$	0.3	650	0.1
Outer halo	$(135–55) \times 27 \times 27$	0.3	20	2.8

radio galaxies, the best fit to the emission line ratios is achieved for log U=−2.5 (McCarthy 1993, McCarthy et al. 1990a). A similar number is obtained in 3C quasars where Q is known (Crawford & Fabian 1989, Crawford et al. 1988). Thus, assuming log U=−2.5 at a characteristic radius in the inner halo of ∼25 kpc gives a density $n_e \sim 3\,\mathrm{cm}^{-3}$. However this assumes the ionizing radiation is emitted isotropically. If photoionization is anisotropic within a cone of opening angle ∼45°, the ionizing flux and corresponding densities are an order of magnitude higher.

We note that the derived densities are only crude estimates due to the many uncertainties (e.g. filling factor and minimum pressures) and can therefore be only order of magnitude estimates.

4.2. Morphology and kinematics of the Lyman α halo

We shall discuss the kinematics of the emission line gas for each of the components as defined in Sect. 3.5 separately.

4.2.1. Inner halo

If the gas motion of the inner halo is gravitational in origin, the velocity dispersion would imply a virial mass of $\sim 10^{12}\,\mathrm{M}_\odot$ inside a radius of ∼30 kpc. However, the spatial correlation of the high velocity gas of the inner halo and the radio structure, the low velocity dispersion of the outer halo and the enhanced and accelerated Lyα gas at radio knot B1, suggest that the high velocity dispersion of the inner halo gas is the result of hydrodynamical interactions with the radio plasma. The interaction of emission line gas with the radio source has been suggested earlier as the cause for the high velocity dispersions of the extended emission line gas in high and intermediate redshift radio galaxies and radio loud quasars and there is evidence that radio sources can entrain and accelerate gas (de Young 1981, van Breugel et al. 1985, de Young 1986, McCarthy et al. 1990a, Chambers et al. 1990, Bremer et al. 1995). Calculations by De Young (1986) showed that gas entrainment rate can be up to a few hundred solar masses per year.

The narrow dips, observed mainly on the blue wing of the Lyα profile of the inner halo and at least one extending spatially from the central part to the separate velocity component at B1, are interesting features that deserve some attention. Although we cannot exclude that these features are due to true velocity structure of the line emitting gas, the spatial continuity of one of these dips from the central Lyα to the blueshifted Lyα emission component at B1 indicates that they are probably due to absorption by associated neutral hydrogen clouds. This also indicates that these absorption clouds must be in front of the Lyα emission region and have a minimal spatial extent of $\sim$ 20 kpc.

If the emission line gas is ionized by anisotropic nuclear photoionization as in the unification models of quasars and radio galaxies, the absorption systems seen against the Lyα emission in 1243+036 may be clouds similar to the Lyα emitting clouds, situated outside the cone of ionizing radiation, but in our line of sight to the Lyα gas (van Ojik et al. 1995b; Röttgering et al. 1995a).

4.2.2. Enhanced Lyα at B1

The positional coincidence of the separate velocity component of the emission line gas and the bend in the radio structure at B1 suggests a direct interaction of the radio jet and the Lyα gas, accelerating the gas to its observed velocity. The interaction of the radio jet with the gas could have locally enhanced the Lyα emission. This will be further discussed in Sect. 4.3.

4.2.3. Outer halo

The narrow velocity width (250 km s^{-1} FWHM) of the emission line gas in the outer halo compared to that of the Lyα emission in the inner halo and its extent to far beyond the radio source supports the suggestion that this very extended component is not affected by the interactions that have stirred up the inner Lyα gas, as mentioned above. The velocity shear observed in the outer halo of $\sim 450\,\mathrm{km\,s}^{-1}$ may be due to rotation or a flow of gas, i.e. infall or outflow. We will discuss these possibilities and their possible connections and implications for the formation of powerful radio galaxies in the early Universe.

(a) Rotation. The velocity shear might be due to a large scale rotation of a gas disk in the halo. A gravitational origin of the rotation of such a large disk implies a mass of $\sim 10^{12}\,\sin^{-2}(i)\,\mathrm{M}_\odot$, where i is the inclination angle of the disk with respect to the plane of the sky. Baum et al. (1992) propose that at low redshifts rotation of the extended emission line gas in powerful radio galaxies indicates the presence of dynamically young disks of gas acquired in a recent interaction or merger with a gas-rich galaxy. These rotating emission line regions are, however, only on scales of ∼20 kpc, while in 1243+036 the outer

halo is almost an order of magnitude larger. Large gaseous halos are common around HZRGs (McCarthy 1993) and may imply that all primeval galaxies in the direct (cluster) environment of HZRGs also possessed such large halos. An interaction between two (primeval) galaxies with large gaseous halos may leave kinematical signs of the event over a much larger scale than the relatively small rotating emission line nebulae that exist around radio galaxies at low redshifts that according to Baum et al. (1992) are due to interactions. Thus, it is possible that the rotating outer halo of 1243+036 originates from an interaction with a neighbouring primeval galaxy.

Alternatively and perhaps more likely, the outer halo Lyα emitting gas in 1243+036 may be a relic of the gaseous halo from which the galaxy has been forming since before the radio source switched on. A rotating disk may have formed during the accretion of gas from the environment. Numerical simulations by Evrard et al. (1994) of the formation of galaxies in hierarchical clustering scenarios indicate that rotating disks with radii of several tens of kiloparsecs naturally form during the formation of galaxies at high redshift ($z = 9$–1).

Note that, although the gas disk does not have to be rotating exactly along the radio axis, it must be within the cone of ionizing radiation from the AGN (if it is anisotropically ionized) and, more importantly, it must be within the slit of the spectrograph that was oriented along the radio axis. The slit has a width of 17 kpc at the redshift of 1243+036. Assuming that a rotating gaseous disk would not be wider than 35 kpc (one quarter of its observed diameter) at a radius of 10″ from the nucleus, this limits the difference between the orientation of the disk and the radio axis to less than 20°.

The fact that we do not see evidence for a disk in absorption against the bright central Lyα emission does not argue against the explanation of the velocity shear as originating from a rotating gas disk. If the observed Lyα gas in the outer halo is ionized by anisotropic nuclear radiation, we would only expect to see the rotating gas disk in absorption against the bright central Lyα if we saw the disk edge on. The size (in the direction of PA2) of the bright central Lyα emission region ($\sim$ 5 kpc) implies an angle between the orientation of the disk and our line of sight of at least 4°.

At first glance, it may seem surprising that in the case of 1243+036 the rotation axis of the gas disk is perpendicular to the radio source axis, because it is generally believed that radio galaxies have a central black hole fuelled by an accretion disk in the inner parts of the galaxy that has its rotation axis along the black hole's spin axis and the radio axis. Thus, the the rotation of the outer halo in 1243+036 cannot be a direct extension of the inner accretion disk. However, there need not be any coupling between the rotation axis of the black hole and the rotation axis of the outer halo. The enormous difference in scale between the two and the complicated way in which accreted matter makes its way to the central few parsecs suggests that matter in the innermost region of the galaxy would have little memory of the rotation axis at 100 kpc. In contrast to this, however, West (1994) notes that there are sometimes remarkable alignments between radio axes of relatively close pairs of powerful radio galaxies, and also between the major axes of neighbouring clusters and their central galaxies. He suggests that this may be a signature of structure formation in the universe from the largest scale structures down to the scales of the most massive galaxies in clusters. In this case the preferred axis for structure formation is the line between neighbouring systems. Röttgering et al. (1996b) find an excess of galaxies along the radio axis of powerful radio galaxies. The orientation of the outer Lyα halo in 1243+036 along the radio axis, would then fit into this scenario of a connection between the (radio) axes of massive galaxies and large scale structure formation.

(b) Outflow. In the case of outflow, it is unlikely that the gas would advance through the extragalactic medium faster than the radio lobes. Therefore, the outflow of gas would need to have existed long before the observed radio source switched on. With the maximum velocity of the most extended emission ($\sim 250\,\mathrm{km\,s^{-1}}$) it would take $\sim 3 \times 10^8$ years to transport the gas out to a radius of 70 kpc, an order of magnitude longer than the most plausible age of the radio source ($\sim 10^7$ years, based on the projected radio size and a radio lobe propagation speed of $\sim 3000\,\mathrm{km\,s^{-1}}$, see Carilli et al. 1991 and references therein). However, we may simply see the galaxy during its most recent period of activity and it may have developed an extended radio source several times during previous active periods in the time needed for the outflow to build up the outer Lyα halo. In that case the outer halo may be gas swept up and deposited by expanding radio lobes during earlier active periods of the galaxy.

Possibly, 1243+036 may have had an active nucleus before its radio activity, ejecting gas along the central black hole's rotation axis. There is evidence for bulk mass outflow of ionized gas close to the nucleus of quasars at velocities up to $1000\,\mathrm{km\,s^{-1}}$ (Carswell et al. 1991). In broad absorption line QSOs even much higher outflow velocities are observed (e.g. Turnshek et al. 1988; Turnshek 1988). However, there have not previously been indications that such outflows originating from the AGN might continue at lower velocities out to distances of 70 kpc. Therefore, we regard it as unlikely that gas ejection by the AGN is the origin of the outer halo of 1243+036 and its velocity shear.

An alternative outflow mechanism may be an equivalent of the 'superwinds' observed in low redshift strong IRAS galaxies (e.g. Heckman et al. 1990; Heckman et al. 1993). These outflows are believed to be caused by a massive starburst in the galaxy. In the burst of star formation, the kinetic energy supplied by stellar winds and supernovae results in the expulsion of interstellar material into the surrounding medium, and can drive a large scale outflow. Some ultraluminous IRAS galaxies (e.g. Arp 220, Mrk 266) have superwinds producing emission line nebulae several tens of kiloparsecs in size (see Heckman et al. 1993 and references therein). Linewidths and observed outflow velocities of emission line gas in the superwinds are typically a few hundred kilometres per second, similar to what we find for the velocity shear and width of the Lyα emission in the outer halo of 1243+036. If a superwind is responsible for the presence and kinematics of the outer halo Lyα gas in 1243+036, then the timescale of the outflow would mean that

a massive initial starburst must have occurred long before the radio source switched on. Heckman et al. (1990) showed that an outflow velocity $v_{100} = 100\,\mathrm{km\,s^{-1}}$ at a radius r kiloparsec with a density of the ambient medium n_{ext} requires a constant energy injection rate $dE/dt \approx 3 \times 10^{41} r^2 v_{100}^3 n_{\mathrm{ext}}$. To produce this energy injection rate by a starburst requires a star formation rate SFR$\sim (dE/dt)/(2.7 \times 10^{41}\,\mathrm{erg\,s^{-1}})\,\mathrm{M_\odot\,yr^{-1}}$. The velocity shear and extent of the outer halo in 1243+036 implies an energy injection rate of $\sim 10^{45}\,\mathrm{erg\,s^{-1}}$ during a period of the halo's dynamical timescale of $\sim 3 \times 10^8$ years. If this energy injection rate is indeed produced by a starburst, it implies a star formation rate for 1243+036 of $\sim 3000\,\mathrm{M_\odot\,yr^{-1}}$ assuming a Salpeter IMF (Heckman *et al.*, 1990 and references therein). A starburst that is biased towards more massive stars may still require $1000\,\mathrm{M_\odot\,yr^{-1}}$, an order of magnitude more than derived for Arp220 (Heckman et al. 1990). Over the dynamical timescale of the outer halo, the entire stellar population of a massive galaxy would have formed. Such a large population of young hot stars could account for the photoionization of a large part of the Lyα gas. In general it is not clear whether the spectral energy distribution of distant radio galaxies allows these star-formation rates. Chambers et al. (1990) derived for 4C41.17, which has a similar R–K color to 1243+036, that the SED only allows such high star-formation rates if there is a large amount of dust present. Other models explaining the SED indicate star formation rates of typically only a few hundred $\mathrm{M_\odot\,yr^{-1}}$.

(c) Infall. The Lyα gas of the outer halo might be infalling gas from the outer parts of the proto-galactic halo. If the radio source associated with 1243+036 is oriented at some angle to the plane of the sky, gas infalling along the radio axis and anisotropically ionized by the AGN could show a velocity structure similar to that observed for the outer halo Lyα gas. However, the radio polarization data of 1243+036 show that the southern radio structure is the least depolarized. If 1243+036 is embedded in a magnetoionic halo, as appears to be the case for most radio galaxies and quasars (Laing–Garrington effect, Garrington et al. 1988; Laing 1988a; Carilli et al. 1994), the southern radio jet should be on the side closest to us. The radiation from the southern part of the radio source has then traveled a shorter distance through the magnetoionic halo than the the northern radio emission and is therefore the least depolarized. This orientation is further supported by the blueshifted Lyα component at the position of the southern radio knot B1, probably caused by the interaction of the radio jet and the gas (see Sect. 4.3). Therefore, it seems somewhat surprising that ionized gas falling in from large radii on the southern side is also blueshifted with respect to the systemic Lyα and not redshifted. Thus, the most likely orientation of the radio axis with respect to the plane of the sky argues against the outer halo Lyα emission being due to infall along the radio axis. Nevertheless, we will consider whether an inflow mechanism could produce the outer halo in 1243+036.

There is much evidence that powerful radio galaxies at high redshifts reside in clusters (e.g. Hill & Lilly 1991 and references therein), and that they have a hot ($\sim 10^7$ K) "cooling flow" intracluster medium (e.g. Cygnus A, Arnaud et al. 1984; 3C295, Henry & Henriksen 1986; 3C356, Crawford & Fabian 1993; see also Fabian 1994; Carilli et al. 1994). Our determination of the minimum pressures and polarization measurements of the radio structure of 1243+036 support this idea (see Sect. 4.1). If the cooling time of that gas is short compared to the age of the Universe at the observed epoch then there will be a cooling flow, depositing cold gas near the centre of the halo. At low redshifts the cooling time of the hot ICM in many clusters is shorter than the Hubble time and therefore gas is cooling and deposited, possibly forming emission line clouds. In nearby cooling flows mass deposition rates up to several hundred $\mathrm{M_\odot\,yr^{-1}}$ have been deduced (see Fabian 1994 and references therein).

The mass of the *ionized gas* in the outer halo of 1243+036 in the observed area that was covered by the slit in orientation PA1, is of order $10^8\,\mathrm{M_\odot}$ (see Sect. 4.2). In the case of a cooling flow, the gas has no preferential direction of infall, so that it is not only along the radio axis (slit orientation PA1), in the ionization cone from the AGN, but roughly isotropically distributed around the radio galaxy. Thus, the total mass of cold ($\sim 10^4$ K) gas in the outer halo all around the galaxy is minimally of order $10^9\,\mathrm{M_\odot}$, situated at a radius of $\sim$60 kpc. If the ionized gas represents only a fraction of the total mass, the total amount of gas in the outer halo may be even an order of magnitude higher. At the redshift of 1243+036 the cooling time would have to be shorter than 10^9 years (the approximate age of the Universe at that epoch) to allow a cooling flow to be the origin of the emission line gas. From an estimated density of $0.1\,\mathrm{cm^{-3}}$ at a radius $\sim$10 kpc (see Sect. 4.1), temperature $T \sim 10^7$ K and the cooling function from Thomas (1988), the cooling time is $\sim 10^8$ years. The density in a hot halo decreases with radius at a rate between r^{-1} and r^{-2}, and the cooling time increases as n^{-1} with constant temperature (Thomas 1988). Then at r = 60 kpc the cooling time is longer than in the inner part of the Lyα halo, but is still $\sim 10^9$ years. Thus it may be possible that a massive cooling flow has deposited a large amount of gas in the outer halo of 1243+036.

A problem for the cooling flow hypothesis is the large velocity shear of the outer halo. In a cooling flow, this is expected to be only a few tens of kilometres per second (Fabian 1994; Fabian et al. 1987), an order of magnitude smaller than that observed in 1243+036. A flow velocity of only $20\,\mathrm{km\,s^{-1}}$ means a mass deposition rate of $\sim 1000\,\mathrm{M_\odot\,yr^{-1}}$ within a radius of 60 kpc, assuming a density of $0.1\,\mathrm{cm^{-3}}$. Fabian et al. (1987) suggests that galaxy interactions are most likely to cause large velocities and Keplerian motion of the gas deposited by a cooling flow. Thus even though a cooling flow may be at least in part responsible for the presence of the emission line gas in the outer halo of 1243+036, it cannot explain the observed velocity shear. An additional mechanism, e.g. a galaxy interaction is needed to account for that. However, unless our arguments about the orientation of the radio source are wrong, i.e. the enhanced, blueshifted Lyα at the projected position of bending point B1 is coincidental and the polarization asymmetry is due to some extraordinary geometry of the magnetoionic halo, we regard the infall of gas as the most unlikely explanation of the velocity shear.

(d) Summary. In summary, we think that rotation due to accretion of gas associated with the formation of the galaxy is the most plausible origin for the presence and kinematics of the outer halo, but outflow in the form of a 'superwind' may also be feasible. A cooling flow may contribute to the presence of the gas but cannot be the cause of the velocity shear. Infall in general seems excluded by the most likely orientation of the radio source. Regardless of the actual origin of the gas in the outer halo and its velocity shear, it is clear that it must have been there since before (the currently active period of) the radio source switched on.

Baum et al. (1992) classified low redshift radio galaxies on the basis of the kinematics of the emission line gas into "rotators", which Baum et al. associate with mergers, "calm non-rotators", identified with cooling flows, and "violent non-rotators", where any organized motion of the emission line gas is overshadowed by interaction with the AGN. 1243+036 shows the presence of two of the kinematical characteristics of the low redshift radio galaxies: a calm rotator in the region outside the radio source and a violent non-rotator in the inner parts. Thus, we may in 1243+036 be witnessing an important stage in the evolution of massive galaxies in the early Universe. The scenario would be that a large scale rotating gas disk or outflowing gas is ionized by the strong continuum emission from the AGN, while the interaction of the radio source with the gas causes large velocities removing signs of the earlier calm kinematics as the radio lobes propagate outwards. In the outer halo, where the gas is still unaffected by the radio plasma, the rotating gas disk is still intact.

We note that in other high redshift radio galaxies a strong extended H I absorption feature against the Lyα is frequently observed (van Ojik et al. 1995b; Röttgering et al. 1995a). These absorption features have velocity widths of a few hundred kilometres per second and absorb a part of the emission line profile over the entire Lyα spatial extent along the radio axis. They may be caused by high column density ($\sim 10^{19}$ cm $^{-2}$) H I absorption systems with a Doppler parameter $b \sim 50\,\mathrm{km\,s^{-1}}$) or by a superposition of many lower column density clouds with an integrated velocity dispersion like that observed of these absorption features. If the latter explanation is the case, the similar velocity width of the strong absorption features observed in some HZRGs and of the Lyα emission from the outer halo in 1243+036, suggests that these features may have a similar origin.

Finally we note that the low surface brightness of the Lyα emission from the outer halo of 1243+036 is of a similar level to that occasionally observed from the extended nebulosity around radio quiet quasars (e.g. Bremer et al. 1992b) and from some damped Lyα absorption systems (e.g. Pettini et al. 1995). Perhaps this represents the quiescent state of the gas around primeval galaxies in general, unaffected by interaction with radio plasma.

4.3. The bent radio structure and its relation with the Lyα gas

Several authors have discussed multiple hotspots and bending of the radio jet in quasars and radio galaxies (e.g. van Breugel et al. 1985; Lonsdale & Barthel 1986a and 1986b; Cox et al. 1991; Icke 1991). An important feature of the bending of the radio jet in 1243+036 is the coincidence of enhanced Lyα emission that is at a blueshifted velocity with respect to the rest of Lyα emitting gas, suggesting a direct interaction between the radio jet and the emission line gas. Line emission at the position of a sudden bend in the radio jet is also seen at low redshift in 3C 277.3 (Coma A) (van Breugel et al. 1985). We will consider three possibilities for the bent radio structure in 1243+036.

4.3.1. Jet deflection by a gas cloud

Lonsdale & Barthel (1986a) argue that the double hotspots often observed in powerful radio sources are due to deflection of the radio jets by a gas cloud. They find that a straight deflection by a dense wall of a massive cloud would be possible, but not very appealing, because very large cloud masses are required ($>10^9\,\mathrm{M_\odot}$). Also, the jet would quickly eat into the wall so that the deflection direction would change more rapidly than the necessary time to build up the secondary hot spots.

Lonsdale & Barthel (1986a) find that the best possible method of deflection might be through a "DeLaval" nozzle (e.g. Blandford & Rees 1974). The jet eats into a cloud, where it inflates a plasma–bubble. The bubble breaks out at the weakest spot in the asymmetrically confining cloud, creating the "DeLaval" nozzle. This then produces collimated outflow that feeds the secondary hotspot. They claim that the cloud with bubble structure will have a long lifetime such that the deflection direction is maintained stationary over the time required to build up the secondary hotspots ($\sim 10^6$ years). The mass and density of the deflecting cloud must be sufficiently large such that it is not blown away past the secondary hot spot.

From the total luminosity of 1243+036, the average energy supply rate to the hot spots is unlikely to be larger than $\sim 3 \times 10^{45}\,\mathrm{erg\,s^{-1}}$ (see Table 3). From this and the total minimum energy of component B4, we estimate that the time to build up component B4 is 10^5–10^6 years (see also Lonsdale & Barthel 1986a). Thus, the advance speed (v_h) of hotspot B1 must be $< 0.01c$ so that B1 does not pass the other hotspots within that time. From minimum energy density (u_h) for B1 in the ram-pressure balance equation $v_h = u_h^{1/2}(3n_{cl}m_{\mathrm{proton}})^{-1/2}$, the density of the deflecting cloud must be $> 0.1\,\mathrm{cm^{-3}}$ (see also Table 4), similar to what Lonsdale & Barthel (1986) derived. This $0.1\,\mathrm{cm^{-3}}$ density gas represents the hot halo as suggested earlier and is sufficient to provide the necessary time to build up the secondary hotspots. As this hot gas most likely uniformly surrounds the whole system it does not itself deflect the radio jet. It must be an overdensity of hot and cold gas, e.g. emission line gas, that deflects the radio jet. This whole region would then be accelerated by the interaction and we shall refer to it as the deflecting "cloud".

The deflecting cloud must be larger than the size of the total working area of the radio jet, i.e. the primary hotspot. The hotspot B1 is unresolved in our 8 GHz maps, i.e. smaller than 1.5 kpc. The size of primary hotspots in powerful radio sources is typically 1 kpc (e.g. Laing 1988b). Assuming that the deflecting cloud has a diameter of ~4 kpc, similar to the determined for the enhanced Lyα emission region at B1, and that it is spherical, the minimal density gives a total mass of $\sim 10^8$ $M_\odot$. The Lyα flux of the region of enhanced emission at the position of B1 indicates the presence of $\sim 10^7$ $M_\odot$ of ionized gas (see Table 5). If the emission line clouds have dense neutral cores then the total mass of gas (neutral and ionized) may be an order of magnitude higher.

Numerical three-dimensional simulations of jet collisions with dense clouds by de Young (1991) show that direct collisions with a dense cloud cannot easily deflect a jet, unless the cloud is very robust. However, a smoother density gradient from the intercloud medium to the gas cloud than in the case of a discreet dense cloud used by de Young (1991) may be more effective in keeping the jet collimated. The simulations of de Young (1991) further show that the velocity of a jet decreases by a factor of $\sim$ 10 after deflection, which must have observational consequences. This may be seen in the 'southern jet' of 1243+036, where after the bend at B1 the radio emission from the jet is much stronger and the spectra of components B2, B3 and B4 are increasingly steeper, probably due to due to electron ageing.

The Lyα image and high resolution spectroscopy show that the enhanced emission at the location of radio hotspot B1 has a velocity of $\sim$ 1100 km s^{-1} with respect to the main Lyα gas. To determine whether the interaction with the radio jet could have accelerated the gas we have to estimate the jet power of 1243+036. A rough estimate can be made from the total radio luminosity (see Table 3) and the conversion efficiency factor ϵ, $L_{jet} \sim 10^{46}/2\epsilon$ (e.g. Bridle & Perley 1984), where the efficiency is probably of order 0.1–0.01. Thus a jet power $> 10^{46}$ erg s^{-1} is a reasonable assumption. Alternatively we can estimate the jet power, assuming that the total minimum energy of the radio components is replenished in the synchrotron lifetime, giving $L_{jet} \sim 10^{47}$ erg s^{-1}. A third estimate comes from the jet thrust of a relativistic jet (not to be confused with the hot spot advance speed which is only $\sim 0.01c$), Π_{jet}=$L_{jet}(\gamma + 1)/(v_{jet}\gamma)$ (Bridle & Perley 1984), that can be determined from the minimum pressure and area of a hotspot. Assuming a hotspot size of 1 kpc (see above) and jet parameters like in Cygnus A, γ = 1.6, $v_{jet} \sim c$ (e.g. Perley et al. 1984), we find $L_{jet} \sim 5\text{x}10^{46}$ erg s^{-1}. Thus it is reasonable to assume that the jet power of 1243+036 is $> 10^{46}$ erg s^{-1}. A gas mass of 10^8 $M_\odot$ with a velocity of 1100 km s^{-1} has a kinetic energy of $1.2\text{x}10^{57}$ erg. The jet can have accelerated this mass over a period of 10^5 years, if the transfer efficiency of jet power to kinetic energy of the gas is ~1%.

In this deflection scenario the pre-existing massive cloud that is hit by the radio jet does not necessarily have to be one kiloparsec-scale cloud, which given the densities of the emission line gas would be Jeans unstable, but could consist of a region of small dense clouds or filaments and low density gas in between. If the clouds are optically thick they can contain large amounts of neutral gas. Whatever bends the radio jet has to be a continuous surface over the working area of the radio jet. Thus, if it is the emission line gas that deflects the radio jet, the clouds must have been turned into a "mist". The interaction with the radio jet may rip apart dense neutral cloud cores forming a gaseous medium with an increased filling factor and covering fraction (Bremer et al. 1996). This "mist" could be the medium in which the De Laval nozzle forms by which the radio jet is deflected The larger filling factor will cause a larger fraction of the gas to be exposed to the ionizing radiation. This will enhance the Lyman α emission from the region. Local shock ionization due to the impact of the jet may further enhance the Lyα emission.

Alternatively Icke (1991) showed that a jet can be bent smoothly by a pressure gradient and thus may bounce off a gas cloud. In the case of 1243+036 the redirected jet would then have several emission knots due to weak shocks from further interactions with the emission line gas. Although this might account for the observed radio structure of 1243+036 and the acceleration of emission line gas at B1, it is not clear if this mechanism would also cause the enhanced Lyα emission from the deflecting cloud.

The dense region that deflects the radio jet might also be to a small gas-rich galaxy moving near the main galaxy. Its observed velocity would then not necessarily be caused by the interaction with the jet, but the small galaxy would deflect the radio jet. This interaction and ionizing radiation from the main galaxy would then cause enhanced Lyα emission from such a system.

4.3.2. Precessing radio jet

An alternative explanation for the bent radio structure with multiple hotspots might be precession of the radio jet. The direction of the southern jet and the slight northern extension of radio lobe A give the radio source an overall Z–shape, suggesting that the jet may be rotating. As the tip of the jet moves over the wall of the radio lobe it would create new hotspots, as in the "dentist's drill" model of Scheuer (1982). The spectral steepening towards the outer parts of the radio structure could be the result of synchrotron aging in older hot spots. But it could also result from there being weaker shocks with distance along the jet in the deflected flow model. Our crude estimate of the synchrotron age of hotspot B4 of 10,000 years (see Table 3) indicates that if the multiple hotspots are due to the directional change of the radio jet, for B4 still to be visible when B1 is being formed, the jet precession speed would be 0.001° yr^{-1} and the jet would have revolved 27 times within the age of the radio source (~10^7 yr). The projected velocity of the jet impact site from B4 to B1 (10 kpc) would be 3c. At these precession speeds we would not expect the jet to be straight from the core-jet component to B1 (and A1) and a straight line of hotspots from B1 to B4, but a more gradually bent S–shape structure. Also at this precession speed the time that the jet feeds the area of one hotspot is a factor 100–1000 shorter than the time required to build up the hotspot (see above). Nor would it have time to accelerate the emission

line gas at B1 to its observed velocity. Even if we have underestimated the age of B4 by a factor of 10, the inferred speeds seem implausibly high.

Thus, we regard the idea of a precessing jet causing the bent radio structure and multiple hotspots as very unlikely. Also the magnetic field projecting along the southern jet (Fig. 7) is consistent with flux freezing and shear flow along the jet (Begelman et al. 1984), and hence supports the idea of a deflected flow model.

We see the bent radio structure projected on the plane of the sky. However, the bending of the southern jet may have taken place partly into the direction of the line of sight. If the jet is still moving relativistically after the deflection, Doppler boosting may increase the observed flux of weak radio knots along the jet. In the light of the orientation unification scheme for radio galaxies and quasars, 1243+036 would be oriented close to the plane of the sky. If the bending of the jet towards us is as much as it is projected on the plane of the sky ($\sim$ 30 degrees), the southern jet could have been deflected to as close as $\sim$30 degrees from our line of sight. For a relativistically moving jet ($\gamma \sim$ a few) the observed flux could have been Doppler boosted by a factor $\sim$3–15 relative to its original direction. The synchrotron emission associated with weak shocks in the deflected southern jet may have been enhanced forming the observed knots B2, B3 and B4.

4.3.3. Sweeping of the radio jet by the ambient gas

As a third possibility, the sudden bend and overall Z–shape of the radio source may be due to "sweeping" of the radio jet by the ambient medium after the jet has been slowed down in the hotspots B1 and A1. Such a mechanism has also been invoked to explain the linear radio features in some Seyferts and the Z–shape of the low redshift radio galaxy 3C 293 (Wilson & Ulvestad, 1982 , van Breugel et al. 1984) where the radio jets are propagating through a rotating gaseous disk. 1243+036 shows both morphological and kinematical similarities to 3C 293 and 3C 305 (Heckman et al. 1982) where there is evidence for rotation and the radio morphology is Z–shaped. At high redshifts not only 1243+036, but also 4C 41.17 exhibits a radio morphology where the axis defined by the outermost radio components is rotated with respect to the axis defined by the inner components. These morphologies suggest that large scale motion of the ambient medium may have deformed the outer parts of the radio source. The possible rotating gaseous disk of the outer halo in 1243+036 indicates that large scale organized motion is present that may provide the transverse ram pressure (sweeping effect) that is required to bend the radio source to its observed morphology. The velocity shear of the outer halo is consistent with solid-body rotation that, if it is sweeping the radio plasma, would indeed cause the straight radio structure of the "southern jet" in 1243+036. Scaling the calculations of van Breugel et al. (1984) for 3C 293 to the much larger jet kinetic energy of 1243+036 (derived above), requires an average density $\sim 2500\epsilon^{-1}\,\mathrm{cm}^{-3}$, where ϵ is the efficiency of order 0.1–0.01 as mentioned above, to bend the jet over a distance comparable to the jet diameter. Thus, the jet must have lost more than 99.9% of its kinetic energy in the hotspot B1 (and A1), and continue onwards as a light, but still fast jet ($> 10^4\,\mathrm{km\,s}^{-1}$, see van Breugel et al. 1984), to be bent by the ($\sim 20\,\mathrm{cm}^{-3}$) rotating gas of the outer halo. Although we cannot exclude this possibility, it seems more plausible that, with a strong interaction at B1, the jet would be deflected along the lines of scenario (i) than that it would continue at high velocity, but with much less thrust, in the same direction.

Thus, the bending of the radio structure in 1243+036 coinciding with accelerated emission line gas is evidence that the radio jet is deflected by the interaction of the jet with the emission line gas. This supports the idea of Barthel & Miley (1988) that the frequent distortions of radio structures of quasars and radio galaxies at high redshifts are caused by interaction of the radio jet with gas clouds in the environment.

4.4. *Aligned R band continuum*

The R-band continuum morphology of 1243+036 is clearly aligned with the principal radio axis, the line connecting components A, N and B1. This alignment of R-band continuum emission with the radio axis is a commonly observed feature in high redshift radio galaxies (Chambers et al. 1987, McCarthy et al. 1987). In addition to this, 1243+036 also has a low surface brightness continuum component (see Fig. 8), which has the same narrow alignment with the principal radio axis and apparently extends beyond the radio lobes. If this faint extended continuum emission is real, this can have important implications for the interpretation of the alignment effect in high redshift radio galaxies.

One of the first proposed explanations for the "alignment effect" was jet induced star formation Chambers et al. 1987, McCarthy et al. 1987, Rees 1989, Begelman & Cioffi 1989, de Young 1989 where shocks from the radio jet and the overpressured radio lobes would lead to star formation in dense clouds along the direction of the jet propagation. Daly (1992) argues that inverse Compton scattering of CMB photons of the relativistic electrons in the radio plasma could cause the alignment effect at high redshifts. Optical polarization measurements of intermediate and high redshift radio galaxies have indicated that much of the aligned continuum light is polarized, therefore some or all of the light is scattered light from a hidden quasar by dust or hot electrons (Scarrott et al. 1990, Tadhunter et al. 1992, Cimatti et al. 1993, di Serego Alighieri et al. 1993, Cimatti et al. 1994, di Serego Alighieri et al. 1994). This indicates that, although jet induced star formation may play a role, scattering processes are important contributors to the alignment effect.

In 1243+036 we see that the aligned continuum does not follow the radio structure that bends at the position of radio knot B1 into the "southern jet". Instead the optical continuum extends further outwards with the same orientation as the inner continuum, the Lyα "cone" and the principal radio axis. This argues against a direct relation between the optical continuum morphology and the radio jet as required by inverse

Compton models and jet-induced star formation and suggests that the optical continuum orientation is linked to the axis of the AGN. However, in the jet-induced star formation scenario, the extended continuum may be a relic of star formation of along a previous path of the jet, when possibly no bending occurred. Thus, the presence of faint extended optical continuum beyond the radio structure maintaining its alignment with the inner radio structure and the brightest Lyα gas favours the scenario of scattering of anisotropically emitted nuclear continuum light, although it is possible that jet induced star formation played a role at an earlier evolutionary stage of the radio source and currently in the inner parts of the radio galaxy.

A much deeper image is needed to confirm the reality of the faint extended continuum emission.

5. Summary and conclusions

We have found and studied the distant radio galaxy 1243+036 at $z = 3.57$. It has spectacular properties both in the optical and in the radio:

1. The radio source extends over 55 kpc, has a sudden bend and multiple hotspot structure. All components have ultra steep spectra and the radio emission is strongly depolarized.

2. The radio galaxy has strong and extended Lyα and [O III]$\lambda\lambda$ 5007,4959 Å emission. The Lyα emission is aligned with the radio source and shows a clumpy structure. It is characterized by three components: (i) the inner halo inside the radio structure with a large velocity dispersion, (ii) enhanced emission with blueshifted velocity at the position of the bend in the radio structure and (iii) a quiescent outer halo with a velocity shear of 450 km s^{-1} extending over a total diameter of at least 135 kpc, aligned with the inner optical and radio axis.

3. The R band continuum is aligned with the principal radio axis and shows a faint extension slightly beyond the radio structure. This emission does not have a sharp bend like the radio emission but stays aligned with the inner continuum, the emission line gas and the principal radio axis.

We have argued that the observations have the following implications:

(a) The quiescent outer Lyα halo must predate the onset of the radio source. The origin of this gas and its kinematics is probably due to the accretion of gas from the environment producing a large scale rotation, although there is a possibility that it is caused by a massive outflow from the central galaxy.

(b) The interaction of the radio jet with the emission line gas is responsible for the bent radio structure. The jet has accelerated the gas at the interaction to a velocity of 1100 km s^{-1} relative to the rest of the system and may have shred the emission line clouds, locally enhancing the Lyα emission. The bending of the radio structure in 1243+036 coinciding with accelerated emission line gas is evidence that gas clouds may be the general cause of bending in high redshift radio sources.

(c) The large velocity dispersion of the emission line gas inside the radio structure and the low dispersion of the gas outside of it, support the idea that the large velocity dispersions of the emission line gas in HZRGs are caused by entrainment of gas by the radio jet or shocks and turbulence in the radio plasma.

(d) The close alignment of the principal radio axis with the inner Lyα gas and especially with the Lyα from the outer halo argues for photoionization by anisotropically emitted radiation from the AGN.

(e) The extended Lyα emission suggests densities of the emission line filaments of order a few to 100 cm^{-3}. The required confinement of the emission line gas and the radio hotspots along with strong depolarization of the radio emission argue for the presence of a dense (0.1 cm^{-3}) hot (10^7 K) halo surrounding the system.

(f) The extension of the aligned optical continuum emission beyond the radio structure which does not follow the bend in the radio source is an argument against inverse Compton scattering and jet-induced star formation as the cause of the alignment effect in this object. It favours scattering of anisotropic nuclear continuum radiation.

The most likely scenario for explaining our observations is that a large rotating gaseous disk, originating from accretion associated with the formation of the galaxy, is ionized by anisotropically emitted continuum emission from the AGN. The interaction of the radio source with the gas bends the radio jet and causes large velocities in the Lyα halo as the radio plasma propagates outwards. In the outer halo the gas is still unaffected by the radio plasma and the quiescently rotating gas disk is still intact.

Because of its large luminosity and spatial extent, 1243+036 provides an important laboratory for investigating the intrinsic nature of high reshift radio sources and the conditions in the early Universe. Further observations of this object are underway using ground based telescopes and the Hubble Space Telescope.

Acknowledgements. We acknowledge support from an EC twinning project and a programme subsidy granted by the Netherlands Organization for Scientific Research (NWO). We thank Steve Eales and Steve Rawlings for their kindness to obtain a K band image.

References

Alexander P., Leahy J.P., 1987, MNRAS 225, 1
Antonucci R., Miller J., 1985, ApJ 297, 621
Arnaud K.A., Fabian A.C., Eales S.A., Jones C., Forman W., 1984, MNRAS 211, 981
Barthel P.D., 1989, ApJ 336, 606
Barthel P.D., Miley G.K., 1988, Nat 333, 319
Baum S.A., Heckman T.M., 1989, ApJ 336, 681
Baum S.A., Heckman T.M., van Breugel W., 1992, ApJ 389, 208
Begelman M.C., Blandford R.D., Rees M.J., 1984, Rev. Mod. Phys. 56, 255
Begelman M.C., Cioffi D.F., 1989, ApJ 345, L21
Blandford R.D., Rees M.J., 1974, MNRAS 169, 395
Bremer M.N., Crawford C., Fabian A.C., Johnstone R.M., 1992, MNRAS 254, 614
Bremer M.N., Fabian A.C., Sargent W.L.W., et al., 1992, MNRAS 258, 23p
Bremer M.N., Fabian A.C., Crawford C.S., 1996, MNRAS (in press)
Bridle, A.H., Perley, R.A., 1984, ARA&A 22, 319

Carilli, C.L., Perley R.A., Dreher J.W., Leahy J.P., 1991, ApJ 383, 554
Carilli C.L., Owen F.N., Harris D.E., 1994, AJ 107, 480
Carilli C.L., van Ojik R., Röttgering H.J.A., et al., 1995, (in preparation)
Carswell R.F., Mountain C.M., Robertson D.J., et al., 1991, ApJ 381, L5
Chambers K.C., Miley G.K., van Breugel W., 1987, Nat 329, 604
Chambers K.C., Miley G.K., van Breugel W.J.M., 1990, ApJ 363, 21
Charlot S. Fall S.M., 1993, ApJ 415, 580
Cimatti A., di Serego Alighieri S., Fosbury R.A.E., Salvati M., Taylor D., 1993, MNRAS 264, 421
Cimatti A., di Serego Alighieri S., Field G.B., Fosbury R.A.E., 1994, ApJ 422, 562
Cox C.L., Gull S.F., Scheuer P.A.G., 1991, MNRAS 252, 558
Crawford C., Fabian A., 1989, MNRAS 239, 219
Crawford C., Fabian A., 1993, MNRAS 260, L15
Crawford C.S., Fabian A.C., Johnstone R.M., 1988, MNRAS 235, 183
Daly R.A., 1992, ApJ 386, L9
de Young D.S., 1981, Nat 293, 43
de Young D.S., 1986, ApJ 307, 62
de Young D.S., 1989, ApJ 342, L59
de Young D.S., 1991, ApJ 371, 69
di Serego Alighieri S., Cimatti A., Fosbury R.A.E., 1993, ApJ 404, 584
di Serego Alighieri S., Cimatti A., Fosbury R.A.E., 1994, ApJ 431, 123
Eales S.A., Rawlings S., 1993, ApJ 411, 67
Eales S.A., Rawlings S., 1995, ApJ, (submitted)
Eales S.A., Rawlings S., Dickinson M., et al., 1993a, ApJ 409, 578
Eales S.A., Rawlings S., Puxley P., Rocca-Volmerange B., Kuntz K., 1993b, Nat 363, 140
Evrard A.E., Summers F.J., Davis M., 1994, ApJ 422, 11
Fabian A.C., 1994, ARA&A 32, 277
Fabian A.C., Crawford C.S., Johnstone R., Thomas P.A., 1987, MNRAS 228, 963
Ferland G., Osterbrock D., 1986, ApJ 300, 658
Ferland G., Osterbrock D., 1987, ApJ 318, 145
Garrington S.T., Leahy J.P., Conway R.G., Laing R.A., 1988, Nat 331, 147
Heckman T.M., van Breugel W.J.M., Balick B., Butcher H.R., 1982, ApJ 262, 529
Heckman T.M., Armus L., Miley G.K., 1990, ApJS 74, 833
Heckman T.M., Lehnert M., Armus L., 1993, In: Shull J.M., Thronson J.H.A. (eds.) The Evolution of Galaxies and their Environments. Kluwer, Dordrecht, p. 455
Henry J.P., Henriksen M.J., 1986, ApJ 301, 689
Hes R., Barthel P.D., Fosbury R.A.E., 1993, Nat 362, 326
Hill G., Lilly S., 1991, ApJ 367, 1
Icke V., 1991, In: Hughes P.A. (ed.) Beams and Jets in Astrophysics. Cambridge University Press, Cambridge, p. 232
Lacy M., Miley G., Rawlings, et al., 1994, MNRAS 271, 504
Laing R.A., 1988a, Nat 331, 149
Laing R.A., 1988b, In: Meisenheimer K., Röser H.-J. (eds.) Hot Spots in Extragalactic Radio Sources. Springer Verlag, Heidelberg, p. 27
Lasker B., Sturch C.R., McLean B.J., et al., 1990, AJ 99, 2019
Lilly S., 1988, ApJ 333, 161
Lonsdale C.J., Barthel P.D.:, 1986a, AJ 92, 12
Lonsdale C.J., Barthel P.D., 1986b, ApJ 303, 617
McCarthy P., 1989, Ph.D. thesis, University of California at Berkeley
McCarthy P.J., 1993, ARA&A 31, 639
McCarthy P., van Breugel W., Spinrad H., Djorgovski S., 1987, ApJ 321, L29
McCarthy P., Spinrad H., van Breugel W., et al., 1990a, ApJ 365, 487
McCarthy P.J., Kapahi V.K., van Breugel W., Subrahmanya C., 1990b, AJ 1014, 100
McCarthy P.J., van Breugel W., Kapahi V.K., 1991, ApJ 371, 478
Miley G.K., 1980, ARA&A 18, 165
Oke J.B., 1974, ApJS 27, 21
Pacholczyk A.G., 1970, In: Freeman W.H. (ed.) Radio Astrophysics, San Francisco
Perley R.A., Dreher J.W., Cowan J.J., 1984, ApJ 285, L35
Pettini M., Hunstead R.W., King D.L., Smith L.J., 1995, In: Meylan G. (ed.) ESO Workshop on QSO Absorption Lines. Springer Verlag, Heidelberg, (in press)
Rees M.J., 1989, MNRAS 239, 1P
Röttgering H.J.A., 1993, Ph.D. thesis, University of Leiden
Röttgering H.J.A., Lacy M., Miley G.K., Chambers K.C., Saunders R., 1994, A&AS 108, 79
Röttgering H.J.A., Hunstead R., Miley G.K., et al., 1995a, MNRAS 277, 389
Röttgering H.J.A., Miley G.K., Chambers K.C., 1995b, A&AS, 114, 51
Röttgering H.J.A., West M.J., Miley G.K., Chambers K.C., 1996b, A&A, 307, 376
Röttgering H.J.A., van Ojik R., Miley G.K., et al., 1996a, A&A, (in press)
Scarrott S.M., Rolph C.D., Tadhunter C.N., 1990, MNRAS 243, 5P
Scheuer P.A., 1982, In: Heeschen D.S., Wade C.M. (eds.) Extragalactic Radio Sources, IAU Symp. No. 97. Reidel, Dordrecht, p. 163
Scheuer P.A.G., 1987, In: Zensus J.A., Pearson T.J. (eds.) Superluminal Radio Sources. Cambridge University Press, Cambridge, p. 104
Steidel C., Sargent W.L.W., 1987, ApJ 313, 171
Tadhunter C.N., Scarrott S., Draper P., Rolph C., 1992, MNRAS 256, 53p
Thomas P.A., 1988, MNRAS 228, 315
Turnshek D.A., 1988, In: Blades J.C., Turnshek D.A., Norman C.A. (eds.) QSO Absorption Lines. Cambridge University Press, Cambridge, p. 17
Turnshek D.A., Foltz C.B., Grillmaier C.J., Weymann R.J., 1988, ApJ 325, 651
van Breugel W., Heckman T.M., Butcher H., Miley G., 1984, ApJ 277, 82
van Breugel W.J.M., Miley G.K., Heckman T.M., Butcher H., Bridle A., 1985, ApJ 290, 496
van Ojik R., Röttgering H.J.A., Miley, et al., 1994, A&A 289, 54
van Ojik R., Röttgering H.J.A., Miley G.K., Hunstead R.W., 1995, A&A (in preparation)
West M., 1994, MNRAS 268, 79
Wilson A.S., Ulvestad J.S., 1982, ApJ 263, 576